nature microbiology

Article

https://doi.org/10.1038/s41564-026-02544-8

S-layer expansion is mediated by hoop-like cracks in the paracrystalline lattice during *Bacillus anthracis* growth

Received: 24 March 2026

Accepted: 13 October 2026

Published online: 10 November 2026

Check for updates

Chen Zhang [1], Yuanchen Yu[1], Qiwei Yu [2] & David Z. Rudner [1]

Surface layers (S-layers) are paracrystalline protein monolayers that envelop archaea and some bacteria, including *Bacillus anthracis*. S-layer subunits in *B. anthracis* are tethered to the underlying cell wall through glycopolymers that are covalently attached to the peptidoglycan (PG) meshwork. Cell growth in this rod-shaped organism occurs by dispersed PG synthesis throughout the cell cylinder. How the crystalline lattice expands in lockstep with the cell wall has remained unclear. Here, using fluorescently labelled S-layer subunits and high-resolution imaging, we show that S-layer expansion during *B. anthracis* growth is mediated by pervasive hoop-like cracks in the lattice. Pulse-chase experiments reveal two modes of S-layer assembly at these cracks: dispersed and focused. Our data suggest that local pulling forces on the S-layer array generated by dispersed cell wall synthesis and expansion of the underlying PG cause crack formation, with ensuing dispersed and focused synthesis enabling S-layer expansion with bacterial growth.

Surface layers (S-layers) encapsulate most archaea and many bacteria and serve as the outermost envelope layer for these organisms[1,2]. These protein monolayers have been implicated in a myriad of envelope-associated functions, including the maintenance of envelope integrity[3–5], cell shape[6,7], adherence[8], biofilm formation[9] and virulence[10] and even the emergence of multicellularity[11]. In *Bacillus anthracis*, the S-layer is critical for pathogenesis and has been implicated in maintaining shape and integrity[5], enabling adherence[12,13] and modulating the host immune response[6,14]. Importantly, immunization with *B. anthracis* S-layer proteins (SLPs) provides protection in a mouse model of inhalational anthrax[14]. In addition, subcutaneous injection of nanobodies directed against the S-layer has been shown to clear a *B. anthracis* infection in a mouse model[6]. These findings highlight the therapeutic potential of disrupting the S-layer and motivate a more holistic and mechanistic understanding of S-layer assembly.

In most cases, SLPs have a bipartite architecture, with an assembly domain that makes lateral interactions to form the two-dimensional crystalline lattice and a domain that anchors the lattice to the underlying cell envelope[15,16]. In archaea, SLPs are typically anchored to the cytoplasmic membrane via a transmembrane segment or through interactions with a membrane-bound protein[17]. In Gram-negative bacteria, SLPs bind the O-antigen of lipopolysaccharide on the outer leaflet of the outer membrane[18,19]. In Gram-positive bacteria, the SLPs are anchored to the underlying cell wall via secondary cell wall polysaccharides (SCWPs)[20–23] (Fig. 1a). These glycopolymers are covalently attached to the peptidoglycan (PG) matrix at one end and non-covalently interact with the SLP anchoring domain at the other. Cell wall synthesis in rod-shaped bacteria like *B. anthracis* occurs via dispersed incorporation of glycan strands throughout the cell cylinder. How the crystalline lattice expands in concert with the cell wall during growth has remained unclear.

S-layer assembly has been studied most extensively in the Gram-negative bacterium *Caulobacter crescentus* and the actinobacterium *Corynebacterium glutamicum*. In *C. crescentus*, SLPs are principally incorporated into the S-layer at a mid-cell zone where most PG synthesis occurs[24,25]. In the polar-growing *C. glutamicum*, new cell wall synthesis occurs at the cell poles, and SLPs are similarly incorporated into the S-layer at these sites[26]. By contrast, much less is known about S-layer assembly in Gram-positive bacteria. In *Clostridiodes difficile*, immunofluorescence microscopy using antibodies that recognize SLP

[1]Department of Microbiology, Harvard Medical School, Boston, MA, USA. [2]Lewis-Sigler Institute for Integrative Genomics, Princeton University, Princeton, NJ, USA. e-mail: rudner@hms.harvard.edu

variants found that new S-layer assembly occurs at discrete patches along the cell body that appeared to co-localize with new cell wall synthesis, assayed with fluorescent D-amino acids (FDAAs)[27]. It was therefore hypothesized that SLPs are incorporated into the S-layer at specific sites of local PG synthesis. However, a more recent study in which the cell wall was visualized after pulse labelling with FDAAs suggests that *C. difficile* grows via dispersed PG synthesis[28], as observed in rod-shaped bacteria like *Bacillus subtilis*. Finally, a study published over a decade ago used fluorescent protein fusions to the *B. anthracis* SLP Sap and observed large patches of Sap-mCherry fluorescence on the cell surface[29]. Although intriguing, this fusion was only partially functional, making it difficult to draw conclusions. Thus, how Gram-positive bacteria assemble their S-layer remains unknown.

Here we investigated *B. anthracis* S-layer assembly during growth using a functional Sap variant that could be labelled with fluorescent dyes combined with widefield and super-resolution microscopy. We discovered that during cell elongation, hoop-like cracks that are perpendicular to the long axis of the cell are formed throughout the S-layer lattice. Our data indicate that crack formation is due to local pulling forces on the S-layer array that are generated by dispersed PG synthesis and expansion of the underlying cell wall. Two modes of S-layer assembly occur at these cracks: dispersed and focused. Our findings are consistent with a model in which dispersed insertion throughout the cell cylinder involves the incorporation of newly synthesized Sap into the cracks followed by resealing of the crystal lattice. The sealed lattice guarantees that the next crack in the S-layer is equally likely to occur inside or outside the newly assembled material, resulting in dispersed assembly. Our data suggest that the focused assembly mode results from the failure of newly incorporated Sap subunits to seal the crack owing to either insufficient Sap protein or the formation of a grain boundary in the crystal lattice. The formation of a weak seam ensures that it will continue to expand as the underlying cell wall expands. Continuous rounds of fill-in without sealing result in large regions of focused S-layer assembly. Experiments in which we induced de novo assembly of an S-layer raft are fully consistent with this model for S-layer assembly. Collectively, our results provide a mechanistic picture of S-layer expansion during *B. anthracis* growth and provide a framework for S-layer assembly in other rod-shaped bacteria that grow by dispersed cell wall synthesis.

Results

Visualizing the S-layer in live cells using fluorescent dyes

B. anthracis has two SLPs, Sap and EA1, that are growth-phase regulated[30]. Sap is produced during the exponential phase, whereas EA1 is synthesized as cells enter the stationary phase. Accordingly, to investigate S-layer expansion during growth, we focused on Sap. To label Sap subunits using maleimide-conjugated fluorescent dyes, we constructed a strain in which serine 405, located in an unstructured loop in its assembly domain, was substituted with cysteine[31] (Fig. 1b). The *sap*(S405C) mutation, referred to as *sap*^{cys}, was generated by allelic exchange at the native *sap* locus. To assess whether the mutation impaired Sap function, we visualized the cells using phase-contrast microscopy. *B. anthracis* cells lacking *sap* are defective in cell separation[29], forming long septate chains (Extended Data Fig. 1a). The chain length of the *sap*^{cys} strain was indistinguishable from that of the wild type (Extended Data Fig. 1a). Furthermore, the S-layer of the *sap*^{cys} strain was qualitatively similar to that of the wild type as assessed using transmission electron microscopy (Fig. 1c and Extended Data Fig. 1b). To label and visualize the S-layer during growth, *sap*^{cys} cells were collected in the early-exponential phase (OD_{600} ~ 0.15), washed with PBS and then incubated with maleimide-STAR RED for 10 min. Unincorporated dye was removed, and the cells were imaged using fluorescence microscopy. As shown in Fig. 1d, the dye labelled the entire cell surface (Fig. 1d and Extended Data Fig. 1c). Importantly, surface fluorescence was virtually undetectable in wild-type *sap*$^{+}$ cells (Fig. 1d and Extended Data Fig. 1c), indicating that the fluorescence signal was due to Sap^{cys} labelling.

We next monitored the S-layer during growth and the stationary phase (Fig. 1e). The *sap*^{cys} strain was grown in rich medium and at time points along the growth curve; cells were collected, labelled with maleimide-STAR RED and imaged as described above. In early-exponential growth (OD_{600} ~ 0.15), the fluorescently labelled S-layer was largely uniform (Fig. 1f). However, in the mid- and late-exponential phases (OD_{600} of ~0.6 and ~2.8, respectively), we observed unlabelled regions on the cell surface, suggesting that the S-layer array did not fully encapsulate the bacterium. Of the mid-exponential cell chains, ~67% showed at least one unlabelled region, and on average, these regions appeared every ~8.75 µm along the cell cylinder (Supplementary Fig. 1a). In the stationary phase (OD_{600} ~ 6), uniform fluorescent labelling was again observed. Finally, in the late-stationary phase (OD_{600} ~ 11), ~75% of the cells contained at least one unlabelled patch (Fig. 1f and Supplementary Fig. 1b). We reasoned that the dark patches in the late-stationary phase were due to the formation of unlabelled arrays of the EA1 SLP. In support of this idea, Sap^{cys} staining was uniform in the late-stationary phase in a strain lacking *eag* that encodes EA1 (Extended Data Fig. 2c,d). However, the unlabelled regions were still present in the mid- and late-exponential phases in the Δ*eag* mutant (Extended Data Fig. 2d). To investigate whether our labelling method was responsible for the distinct S-layer patterns observed in the mid- and late-exponential phases, we generated a strain in which an ALFA tag was inserted in the same unstructured loop in the assembly domain and visualized the S-layer using fluorescently labelled anti-ALFA nanobodies[32] (Extended Data Fig. 2a,b). As shown in Fig. 1f, S-layer labelling of Sap^{ALFA} was similar to that of Sap^{cys} at all growth phases. We conclude that the absence of Sap^{cys} labelling in discrete regions along the cell surface during the mid- and late-exponential phases is not a labelling artefact and likely reflects the inability of Sap production to keep pace with growth ('Discussion'). Accordingly, to investigate S-layer assembly during cell elongation, we restricted our analysis of Sap^{cys} localization to cells in early-exponential phase (OD_{600} ~ 0.1–0.4).

Analysis of S-layer expansion during growth reveals two modes of assembly

To investigate how the Sap S-layer expands during growth, we labelled *sap*^{cys} cells in the early-exponential phase with maleimide-STAR RED, returned the cells to rich medium after removing unincorporated dye and then imaged the S-layer over time (Fig. 2a). In this 'cold-chase' experiment, all newly synthesized Sap^{cys} protein is unlabelled. Accordingly, any dark regions on the cell surface reflect newly incorporated Sap into the S-layer. We observed two types of unlabelled Sap incorporation: (i) dark bands that grew larger over time and (ii) a reduction in Sap-STAR RED signal throughout the cell surface (Fig. 2a–c and Extended Data Fig. 3). Both required ongoing PG synthesis (Supplementary Fig. 2). We refer to the former as focused assembly and the latter as dispersed assembly and address each mode separately below.

Dark bands were present in the majority of cell chains by 45 min (Fig. 2a and Supplementary Fig. 3) and are consistent with focused and continuous incorporation of unlabelled Sap at specific sites along the cylinder. To investigate whether focused S-layer assembly was due to focused expansion of the underlying cell wall, we labelled the cell wall PG with FDAAs[33] before pulse labelling of Sap^{cys} and then monitored the cell wall and S-layer over time. As shown in Fig. 2a, the FDAA signal decayed uniformly along the lateral wall (Fig. 2a and Extended Data Fig. 3b). Similar results were obtained with a different FDAA dye (Extended Data Fig. 3c). Importantly, dual-colour pulse-chase labelling of the cell wall during growth is consistent with dispersed PG synthesis throughout the cell cylinder (Extended Data Fig. 3d), similar to *B. subtilis* and other rod-shaped bacteria[34]. These results indicate

https://doi.org/10.1038/s41564-026-02544-8

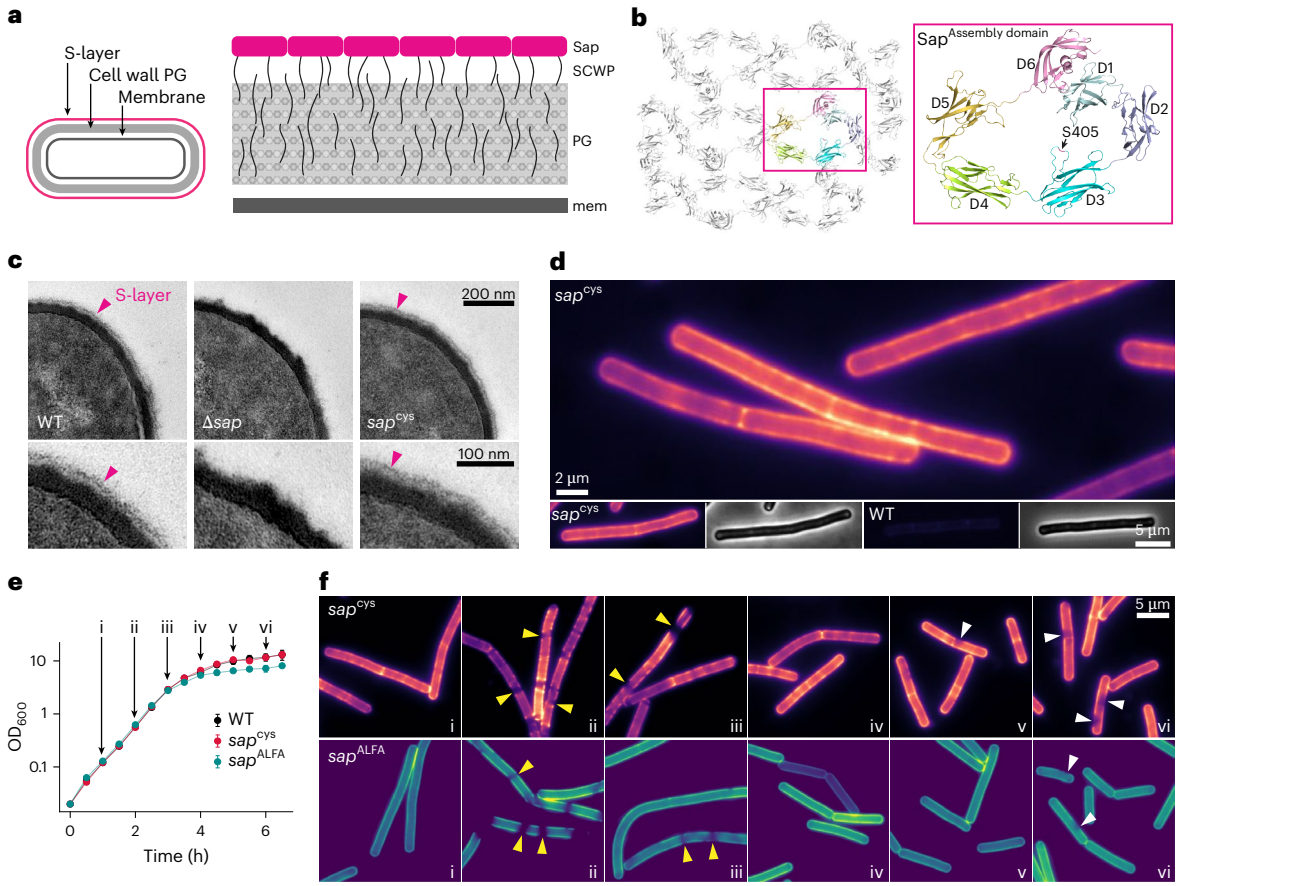


Fig. 1 | Visualizing the *B. anthracis* Sap S-layer. a, Schematic of the *B. anthracis* cell envelope. The Sap S-layer is tethered to the cell wall PG via SCWPs. The cytoplasmic membrane (mem) is also shown. **b**, Structure of an in vitro-grown Sap S-layer lattice (PDB 9G93). The six Ig-like domains (D1–D6) of a single Sap assembly domain are highlighted. S405 in an unstructured loop of the D3 domain is substituted with cysteine in Sap^{cys}. **c**, Representative transmission electron micrographs of the indicated strains. The S-layer (carets) is indicated. WT, wild type. **d**, Representative fluorescence images of the indicated strains labelled with maleimide-STAR RED. Cells in **c** and **d** were collected in early-exponential phase (OD_{600} ~ 0.15). **e**, Growth curves of the indicated strains in rich medium. Data are mean ± s.d. of three biological replicates. Arrows (i–vi) indicate the time points at which cells were imaged in **f**. **f**, Representative fluorescence images of the indicated strains labelled with maleimide-STAR RED (*sap*^{cys}) or anti-ALFA-ATTO488 (*sap*^{ALFA}) at the indicated time points (i–vi). Dark bands on the cell surface in mid/late-exponential phase (yellow carets) and dark patches in stationary phase (white carets) are indicated.

that the focused S-layer expansion is not due to focused PG synthesis. To explore whether the focused S-layer expansion occurred at cell division sites, we visualized the cell membranes and newly incorporated unlabelled Sap^{cys} using time-lapse fluorescence microscopy. Figure 2b shows that the focused S-layer expansion does not specifically occur at division sites (Fig. 2b and Supplementary Video 1). Similar results were obtained using snapshots to avoid phototoxicity during time-lapse imaging (Extended Data Fig. 4a).

Finally, we investigated whether the focused Sap incorporation was due to localized secretion of Sap protein. We generated a functional YFP fusion to the essential SecE component of the SecYEG translocon. The *yfp* gene was fused to *secE* by allelic exchange such that the fusion was expressed under native control. The S-layers of the *yfp-secE* strain and the wild type were indistinguishable based on fluorescence labelling and transmission electron microscopy (Supplementary Fig. 4). Analysis of YFP-SecE using fluorescence microscopy revealed that it localized uniformly in the cytoplasmic membrane throughout growth (Extended Data Fig. 4b–d). Although it is possible that not all YFP-SecE proteins were incorporated into SecYEG translocons or that a subset of translocons function in Sap secretion, the data suggest that Sap is secreted everywhere along the cytoplasmic membrane. Collectively, these experiments suggest that focused S-layer expansion is an intrinsic feature of S-layer assembly ('Discussion').

Next, we investigated the reduction in labelled Sap-STAR RED signal along the entire cell surface during growth—a process we refer to as dispersed S-layer assembly (Fig. 2b). As Sap proteins are anchored to the cell wall and *B. anthracis* sheds its PG during growth[35,36], we first investigated whether the reduction in Sap signal along the cylinder was due to subunit shedding. We quantified the average Sap-STAR RED fluorescence intensity per unit area at each time point during the cold chase. The normalized intensity decayed exponentially with a half-life of ~25 min (Fig. 2d). Importantly, the doubling time of *B. anthracis* under our assay conditions was also ~25 min, suggesting that the reduction in normalized intensity was due to signal dilution as the cell elongates, rather than subunit shedding. In a complementary approach, we analysed the Sap-STAR RED in the culture medium and the surface-associated protein at each time point in the cold chase shown in Fig. 2a (Methods). An identical volume of culture was collected at each time point, and the proteins in the culture medium were precipitated using trichloroacetic acid (TCA). The surface-associated proteins were extracted from the cell pellet using urea, followed by TCA precipitation. The two fractions were then resolved using polyacrylamide gel electrophoresis and visualized using in-gel fluorescence (Fig. 2e). The vast majority of the labelled Sap remained surface associated over the entire cold-chase time course. Thus, the reduction in labelled Sap along the cell cylinder in

https://doi.org/10.1038/s41564-026-02544-8

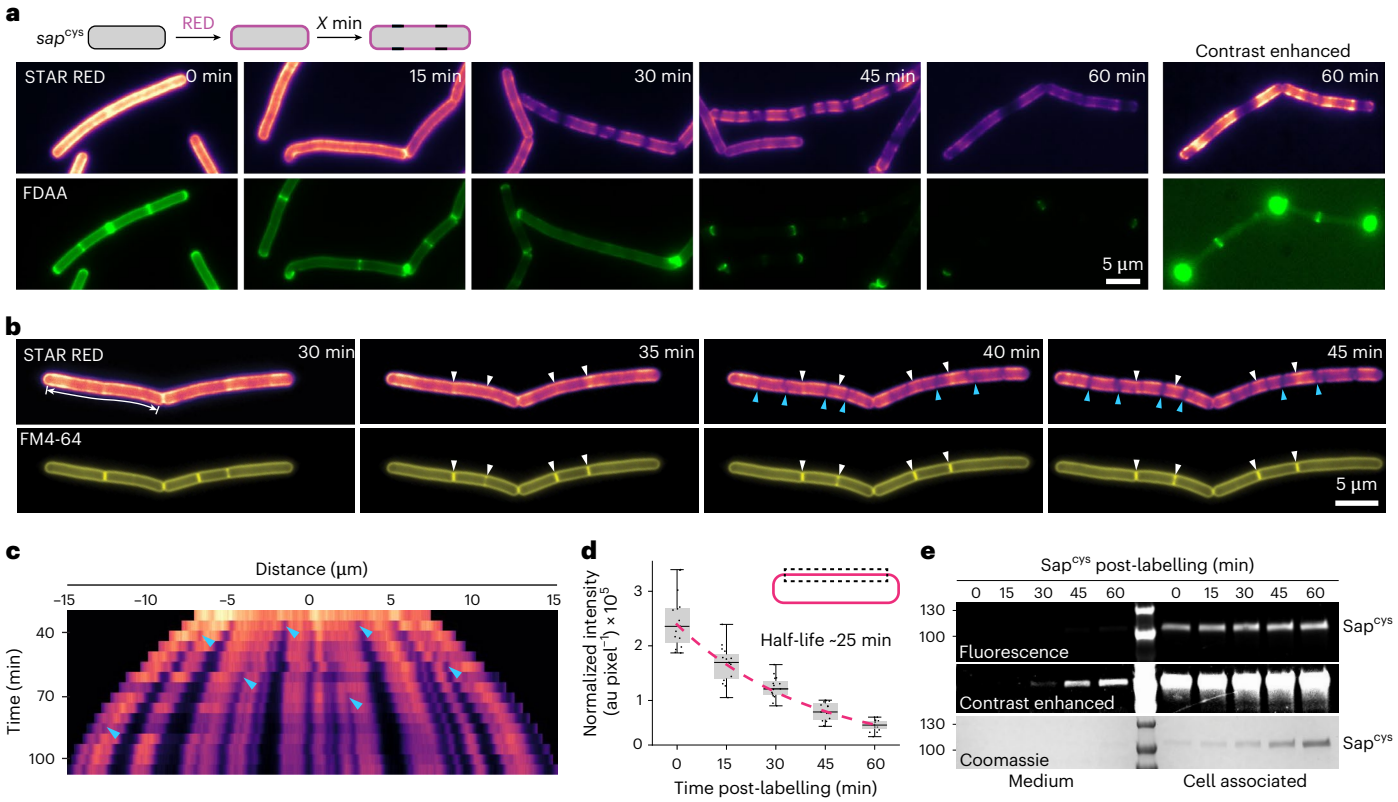


Fig. 2 | Two modes of Sap S-layer assembly. a, Top: schematic of the cold-chase assay. *sap*^{cys} cells were labelled with maleimide-STAR RED, returned to growth medium and imaged at later time points. Bottom: representative fluorescence images of the S-layer at the indicated times after the return to growth. The cell wall PG was labelled with the FDAA ATTO488-D-lysine-NH_2 for 2 h before pulse labelling of Sap^{cys}. The fluorescence images were processed identically with the same min/max intensities applied. Contrast-enhanced images from 60 min after chase are shown to visualize the homogeneous loss of FDAAs along the cell cylinder. **b**, Representative time-lapse images of *sap*^{cys} cells that were pulse labelled with STAR RED at the indicated time points. The cells were continuously labelled with the membrane dye FM4-64. Septa (white carets) and dark bands that lack Sap-STAR RED (blue carets) are highlighted. **c**, Kymograph of time-lapse images of Sap-STAR RED along one side of the cell cylinder (indicated in **b**). Time points when some of the dark regions appeared are highlighted with blue carets. **d**, Normalized Sap-STAR RED intensities along one side of the cell cylinder ($n = 15$ technical replicates per time point) were plotted at the indicated times during the cold chase. Data are presented as boxplots where the minimum, maximum, centre and bounds of each box indicate the lowest, highest and median (50th percentile) values, and interquartile range (IQR; 25th to 75th percentile) of the data, respectively. Lower and upper whiskers extending from the edge of each box indicate 1.5× the IQR range. The pink dashed curve represents an exponential decay fit of the raw data. Similar results of the intensity decay were obtained in three biological replicates. **e**, Representative in-gel fluorescence and Coomassie staining of Sap^{cys} protein present in the culture medium or extracted from the cell surface. The same volume of culture was removed and processed at each time point after pulse labelling. Newly synthesized unlabelled Sap^{cys} during the cold chase accounts for the increase in Coomassie-stained Sap^{cys} over time and serves as a control for loading. Molecular weight markers in kDa are indicated.

our cold-chase experiment likely reflects insertion of unlabelled Sap subunits throughout the S-layer. Collectively, these results reveal two modes of S-layer assembly during growth: Sap subunit insertion throughout the S-layer and focused, continuous insertion at discrete regions along the cell cylinder.

S-layer expansion is mediated by hoop-like cracks

To visualize both the old and newly synthesized S-layer, we performed dual-colour pulse-chase experiments using spectrally distinct dyes (Fig. 3a). Importantly, using 10 µM maleimide-STAR GREEN or CF594, we could label virtually all accessible Sap^{cys} subunits, ensuring that the second dye (STAR RED) used in the chase labelled newly synthesized material (Extended Data Fig. 5a and Supplementary Fig. 5). By contrast, the anti-ALFA nanobodies were unable to bind all accessible Sap^{ALFA} subunits and were therefore not used in these experiments. Figure 3 shows an example of a dual-colour pulse-chase experiment. Sap^{cys} was labelled with STAR GREEN, and the cells were returned to rich medium at an OD_{600} ~ 0.1. At the indicated time points, the cells were collected, labelled with STAR RED and then directly imaged. Similar to the cold-pulse experiments, there were two modes of S-layer assembly. We observed newly incorporated Sap-STAR RED throughout the S-layer as well as focused incorporation in regions that lacked Sap-STAR GREEN (Fig. 3a and Extended Data Fig. 5b). Quantification of the fluorescence intensity after a 30 min chase revealed that focused incorporation per unit length was ~1.8-fold greater than the dispersed insertion (Supplementary Fig. 6). These data are consistent with the idea that the bands of focused insertion consist entirely of new Sap^{cys} subunits, whereas regions of dispersed insertion are composed of old and new Sap^{cys}.

We note that in some of the areas of focused synthesis, we observed unlabelled regions between the old (green) and new (red) Sap S-layer (Fig. 3a, red carets). These dark regions suggested that newly synthesized Sap assembles separately from the older material rather than becoming incorporated into the existing crystal lattice. However, we found that these dark regions are due to the difference in fluorescence intensities of the two dyes and the contrast required to visualize both of them in the merged image. Experiments in which we used the same fluorescent dye for the pulse and chase, with the pulse dye containing a trace amount of the second colour, revealed a continuous S-layer signal spanning old and newly assembled Sap protein (Extended Data Fig. 5c). Thus, the assembly of new S-layer is templated on the pre-existing material. Finally, we observed a few dark regions flanked by newly

https://doi.org/10.1038/s41564-026-02544-8

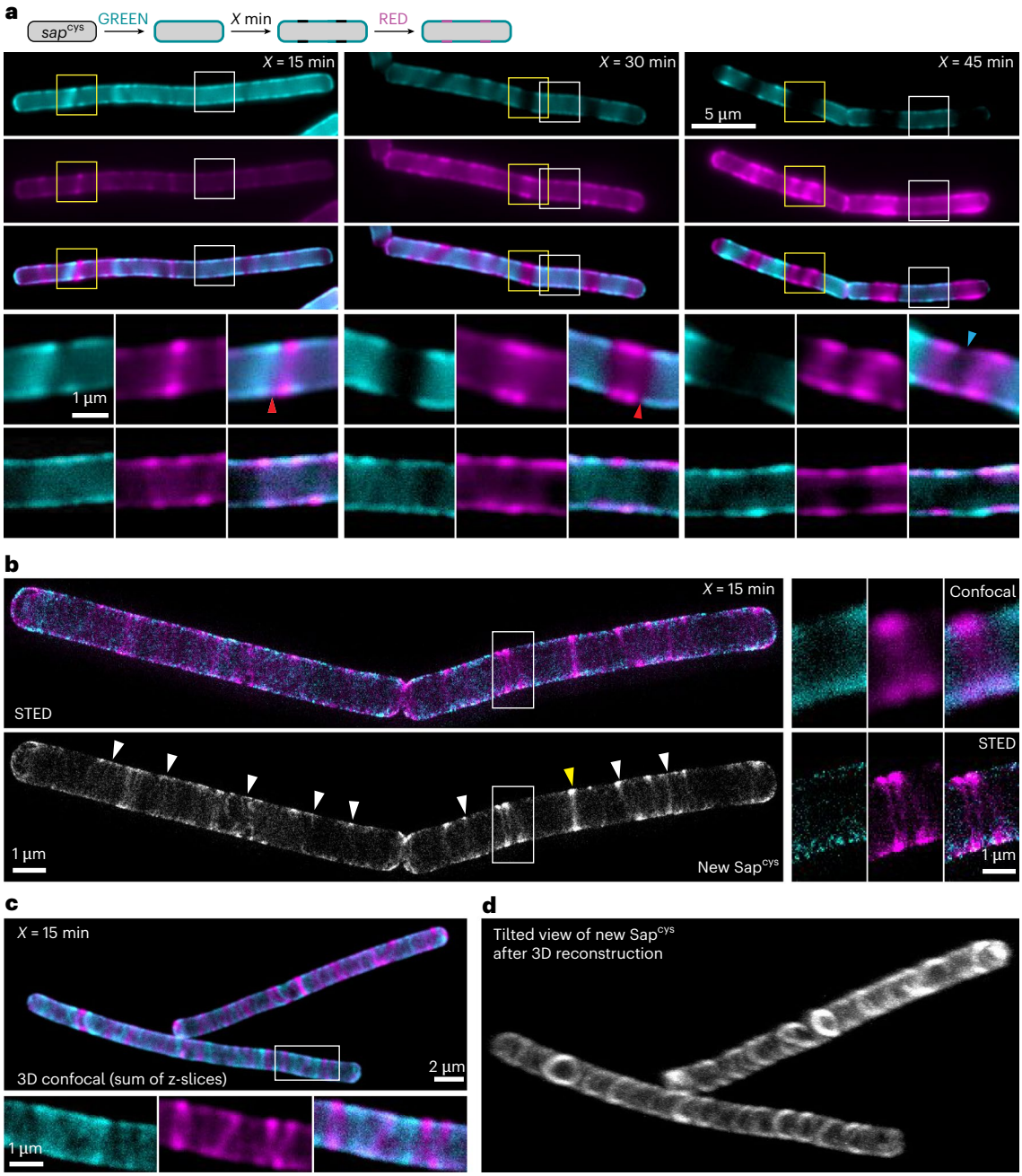


Fig. 3 | Both S-layer assembly modes involve incorporation of new Sap subunits into hoop-like cracks. a, Top: schematic of the dual-colour pulse-chase assay. The S-layer was labelled with STAR GREEN (or CF594 for STED), and the cells were returned to rich medium. At later time points, newly synthesized Sap^{cys} subunits were labelled with STAR RED. Bottom: representative fluorescence images of the S-layer at the indicated times after the return to rich medium. The fluorescence images of individual dyes were processed identically with the same min/max intensities applied. The contrast was adjusted in the merged images to visualize both dyes. Examples of focused (yellow boxes) and dispersed (white boxes) insertion of new Sap-STAR RED are highlighted and enlarged below. Dark regions between green and red Sap (red carets) and between two bands of red Sap (blue caret) are indicated. **b**, Representative STED image of *sap*^{cys} cells 15 min after growth in rich medium. Dual-colour image (top) features both old and newly incorporated Sap subunits. Grey-scale image (bottom) shows new Sap synthesis. Dispersed (white carets) and likely focused (yellow caret) insertions are indicated. Corresponding confocal and STED images of the boxed region are shown on the right. **c**, Representative confocal image of cells 15 min after chase. Sum of z-slices of 3D confocal images features both old and newly incorporated Sap subunits. Enlarged single-colour and merged images of the boxed region are shown below. **d**, Tilted view of the 3D reconstruction of the newly synthesized Sap-STAR RED image in **c**.

synthesized (red) S-layer (Fig. 3a, blue caret). We suspect that these dark regions are real gaps in the S-layer resulting from insufficient Sap production as cells enter the mid-exponential growth phase (Fig. 1f).

To visualize S-layer assembly at higher resolution, we performed a dual-colour pulse-chase and visualized the S-layer using stimulated emission depletion (STED) super-resolution microscopy. After a 15 min chase, we detected faint foci of new S-layer along most of the cell surface in addition to fluorescent lines that crossed the long axis of the cell (Fig. 3b and Extended Data Fig. 6a). We suspect that this localization pattern reflects the two modes of S-layer assembly described above. The faint foci and the thin and faint fluorescent lines reflect dispersed Sap insertion throughout the S-layer, and the thicker fluorescent lines

https://doi.org/10.1038/s41564-026-02544-8

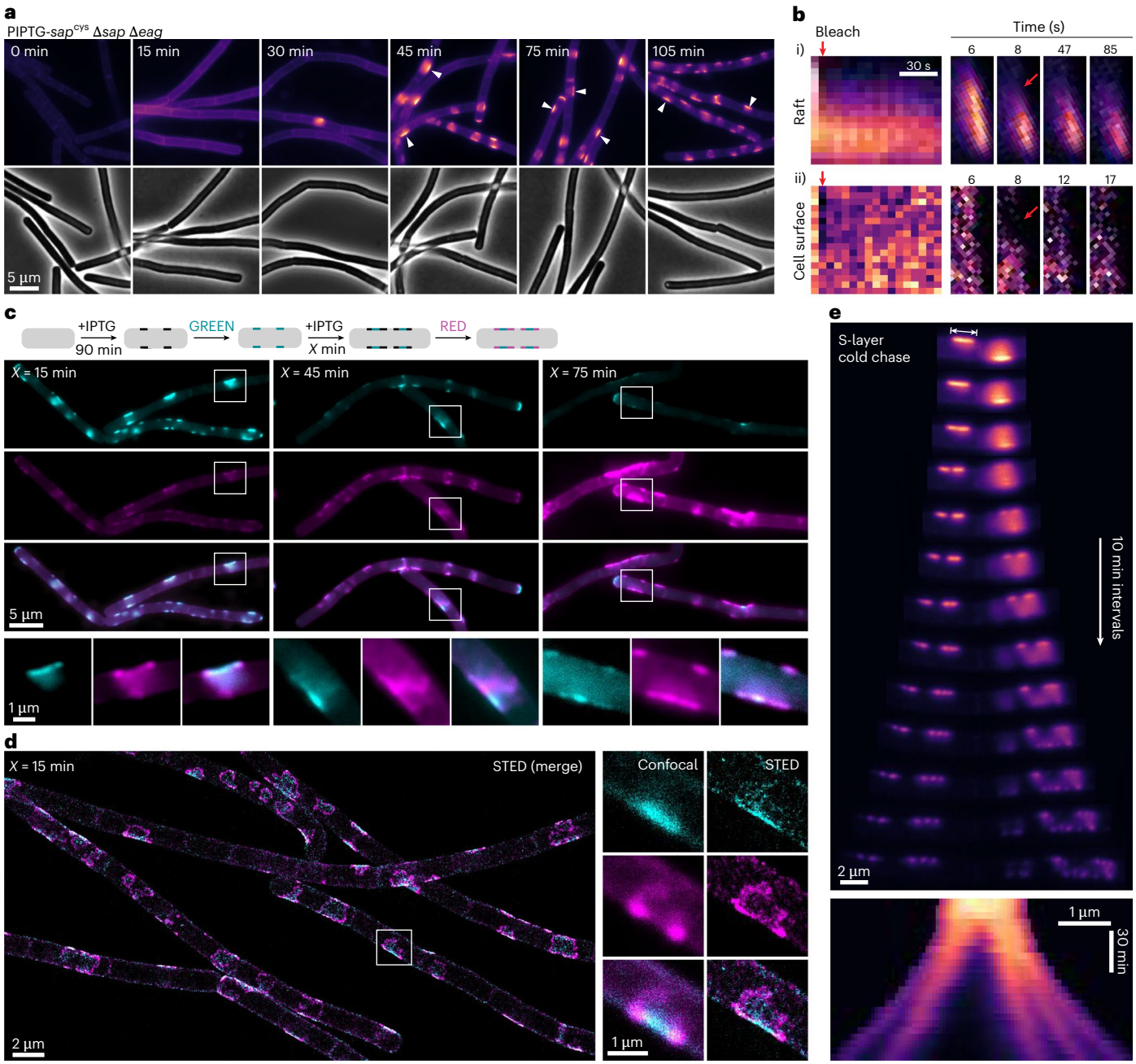


Fig. 4 | S-layer nucleation and cracking revealed from de novo reconstruction. **a**, Representative fluorescence and phase-contrast images of a strain lacking *sap* and *eag* and harbouring an IPTG-inducible allele of *sap*^{cys}. At the indicated times after IPTG addition (0.5 mM), Sap^{cys} was labelled with STAR RED and visualized. Examples of Sap-STAR RED rafts that look like discrete lines on the cell surface are highlighted (white carets). **b**, Kymographs of fluorescence recovery after photobleaching (FRAP) images. A region containing a Sap-STAR RED raft (i) and a region on the cell surface lacking a raft (ii) were imaged before and after photobleaching. Images acquired directly after bleaching are indicated, and red arrows point to the bleached region. A subset of images during recovery are shown on the right. **c**, Top: schematic of the dual-colour pulse-chase assay. After 90 min of Sap^{cys} expression, the cells were labelled with STAR GREEN and then returned to rich medium containing IPTG. At later time points, newly synthesized Sap^{cys} subunits were labelled with STAR RED, and old and new S-layer materials were visualized. The fluorescence images were processed identically with the same min/max intensities applied. Boxed regions are enlarged below with contrast enhanced to visualize both dyes. **d**, Representative STED image of cells 15 min after chase. Dual-colour image features old S-layer (green) and newly incorporated Sap subunits (red). Enlarged confocal and STED images of the boxed region are shown on the right. **e**, Top: representative time-lapse of cells with STAR RED-labelled S-layer rafts grown on a BHI agarose pad supplemented with IPTG. Kymograph of time-lapse images of Sap-STAR RED along one side of the S-layer raft indicated in the top panel.

are the focused insertions at specific sites along the cylinder. Finally, we turned to three-dimensional (3D) confocal imaging to visualize S-layer assembly. As shown in Fig. 3c, this method revealed fluorescent lines that traversed the long axis of the cell that were similar to those observed using STED (Fig. 3c and Extended Data Fig. 6b). Importantly, the tilted view of the 3D reconstructed image revealed fluorescent hoops of newly assembled S-layer material (Fig. 3d and Supplementary Video 2). These findings support a model in which hoop-like cracks in the crystalline lattice are generated during cell elongation and new Sap subunits are incorporated into the array at these positions.

https://doi.org/10.1038/s41564-026-02544-8

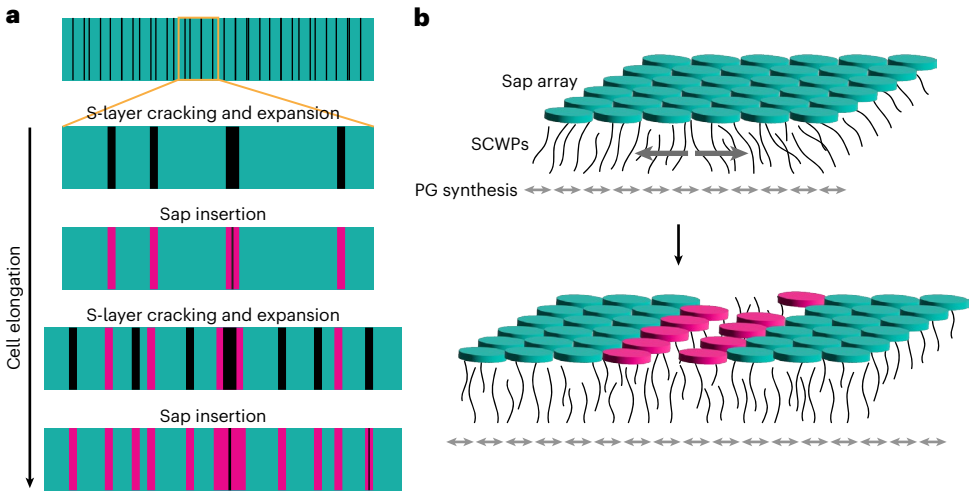


Fig. 5 | Schematic model of S-layer expansion during growth. a, Schematic of the two modes of S-layer assembly. Pervasive hoop-like cracking generates gaps (dark lines) in the lattice (green). The gaps are filled by incorporation of newly synthesized Sap (red lines). The Sap subunits either seal the crack, reconstituting the crystal lattice, or fail to do so. In the latter case, a weak seam in the lattice (thin black line) ensures additional rounds of localized expansion and Sap insertion as the cell elongates, resulting in focused S-layer assembly. In regions where the crack gets sealed, cell growth generates additional cracks that are dispersed throughout the region, resulting in dispersed S-layer assembly. **b**, Schematic of S-layer assembly during growth. Top: dispersed cell wall PG synthesis during growth generates local pulling forces on the S-layer array via SCWP tethers. The pulling forces crack the lattice and drive its expansion. New Sap proteins (red) are incorporated into the S-layer at the edge of the crack.

S-layer nucleation and cracking revealed by de novo S-layer formation

To gain deeper insight into S-layer assembly, we constructed a strain in which we could monitor de novo S-layer formation. We fused the *sap*^{cys} allele to an IPTG-regulated promoter and inserted the fusion at a neutral chromosomal locus in a strain lacking the native *sap* and *eag* genes. We grew the cells in the absence of IPTG, then induced the expression of Sap^{cys} and monitored its localization after labelling with maleimide-STAR RED (Fig. 4a). Before IPTG addition, fluorescent Sap^{cys} was virtually undetectable. After 15 min of induction, the fluorescently labelled protein was observed, albeit faintly, along the entire cell body. However, by 30 min, we detected a few fluorescent patches on the cell surface that increased in number over the next 45 min (Fig. 4a). Many of the Sap^{cys} patches in the widefield images look like discrete fluorescent 'lines' along the cell surface (carets in Fig. 4a), suggesting that the newly synthesized proteins assembled into an S-layer lattice rather than a non-specific aggregate. Experiments described below are consistent with this conclusion. These data suggest that there is a critical concentration of Sap that is required to nucleate an S-layer array, and once nucleated, the array grows in size (0.6–1.2 µm in length) while other nucleation events occur along the cell body. Importantly, fractionation experiments indicate that Sap^{cys} expressed under IPTG control remained cell associated (Extended Data Fig. 7a). These findings suggest that Sap can diffuse along the cell surface until it encounters an array.

To investigate Sap dynamics, we performed fluorescence recovery after photobleaching experiments on the Sap^{cys} fluorescent arrays and on the fainter Sap^{cys} fluorescent signal present throughout the cell cylinder. The bleached region of the S-layer lattice did not recover during the 90 s recovery period (Fig. 4b). However, the labelled Sap^{cys} that was not associated with a fluorescent patch recovered rapidly (<4 s) (Fig. 4b and Extended Data Fig. 7b,c), which likely reflects the movement of Sap subunits on the cell surface, in the PG meshwork and possibly in the periplasmic space between the cytoplasmic membrane and the PG[37]. These data support the idea that Sap proteins diffuse on the cell surface, but once they associate with an S-layer array, they become immobile. Furthermore, the lack of mobility of the fluorescent patch (Fig. 4b) suggests that these patches are stably tethered to the underlying cell wall.

To investigate how the fluorescent arrays are assembled, we performed dual-colour pulse-chase experiments. Sap^{cys} expression was induced for 90 min and then stained with STAR GREEN, unincorporated dye was removed, and the cells were grown in rich medium in the presence of IPTG. At later time points, the newly synthesized Sap^{cys} was labelled with STAR RED, and the S-layer rafts were visualized using fluorescence microscopy (Fig. 4c and Extended Data Fig. 8). Within 15 min of new Sap^{cys} synthesis, we could detect Sap-STAR RED associated with green rafts. The red signal was principally localized at the edges of the array, consistent with the idea that newly synthesized Sap^{cys} diffuses along the cell surface and incorporates into the preformed lattice. At 45 min, we observed gaps in the green fluorescent arrays that contained STAR RED Sap^{cys}. Finally, by 75 min, the green patches were largely replaced by red fluorescence. These findings provide additional support for the idea that the fluorescent patches are indeed S-layer arrays, rather than aggregates, and suggest that the immobile lattice cracks as the cell grows, allowing newly synthesized Sap to fill the gaps. Multiple rounds of cracking and fill-in dilute the old material that is supplemented with newly synthesized red Sap^{cys}.

We used STED microscopy to provide a higher-resolution view of raft assembly. Consistent with the diffusion-and-incorporation model, we found that newly synthesized Sap^{cys} (red) encircled the preformed S-layer lattice (green) (Fig. 4d and Extended Data Fig. 9). To monitor the spatiotemporal cracking of the S-layer raft, we performed a cold-chase experiment and monitored the fluorescent S-layer lattice using time-lapse microscopy. We induced Sap^{cys} for 90 min, labelled the proteins with maleimide-STAR RED and then followed the fate of the labelled lattice over time. During cell elongation, the S-layer raft cracked at multiple sites, and the dark patches that were formed increased in size over time (Fig. 4e and Supplementary Video 3). The cracks and dark patches were strikingly similar to those observed in our cold-chase experiments with the natively expressed Sap^{cys} that fully encapsulated the cell (Fig. 2c). The fragmentation of the S-layer rafts indicates that the pulling forces exerted on the array during growth are local. This suggests that dispersed cell wall synthesis along the

cell cylinder generates local pulling forces that are transduced by the SCWP tethers to the S-layer above.

Discussion

Altogether, our studies reveal that *B. anthracis* S-layer expansion during growth occurs through hoop-like cracks in the paracrystalline lattice that are perpendicular to the long axis of the cell. Our data suggest that these cracks occur along the entire cell cylinder and are mediated by local pulling forces on the S-layer lattice that are generated by dispersed PG synthesis and expansion of the underlying cell wall. The data suggest that the two modes of S-layer assembly, dispersed and focused, initiate with hoop-like cracks (Fig. 5). In the case of dispersed S-layer assembly, we hypothesize that newly synthesized Sap subunits are incorporated into the cracked S-layer, resealing the crystalline lattice. Accordingly, the next crack that occurs is equally likely to occur inside or outside the newly assembled material. We propose that focused S-layer assembly arises from newly incorporated Sap subunits filling in a crack but failing to seal it. This failure could be due to insufficient Sap protein or the formation of a grain boundary that is incapable of sealing and reconstituting the crystal lattice. In either case, a weak seam in the monolayer is produced that will continue to expand as the cell elongates (Fig. 5). Continuous rounds of fill-in without sealing followed by expansion due to cell elongation generate regions of focused S-layer assembly.

Intriguingly, we found that little Sap protein is lost from the S-layer during growth, despite reports of active cell wall turnover as *B. anthracis* elongates[35,36]. We suspect that cell wall hydrolases cleave and release relatively small PG fragments that can diffuse through the S-layer lattice. These fragments would have few SCWP tethers linking them to the S-layer. Loss of the non-covalent interactions between the SCWPs and the Sap subunits that are held in place by lateral interactions within the lattice would result in PG release while leaving the S-layer intact. We envision that a similar loss of interactions between the SCWPs and Sap subunits could occur during S-layer expansion. In these cases, local pulling forces could disrupt these tethers, but neighbouring free and unstrained SCWPs would bind these Sap subunits, securing the lattice in place.

Our de novo S-layer assembly experiments provide additional insight into S-layer expansion. The data suggest that free Sap subunits can diffuse along the cell surface until they encounter and assemble into an S-layer raft. We suspect that these mobile subunits are dimers or small oligomers with two or more SCWP binding sites, enabling movement along the surface while remaining tethered to the underlying PG meshwork. Furthermore, the immobility of the S-layer rafts indicates that once a sufficient number of tethers are formed, the lattice can no longer move. Cracking and movement of these rafts only occur during growth when local pulling forces exerted on a sufficient number of SCWP tethers overcome lateral interactions in the S-layer.

An additional finding in this study that merits discussion is the absence of a Sap array on regions of the cell surface during mid- and late-exponential growth. We propose that Sap production is unable to keep pace with cell elongation during these growth phases. In this model, newly synthesized Sap proteins are incorporated at the edges of a hoop-like crack but are unable to completely fill it. As the cell elongates, this gap in the S-layer continues to expand, generating the dark regions observed in our cold-chase experiments. Evocative freeze-fracture images published in the 1960s revealed crystalline lattices that fully encapsulate the microbe studied[38–40]. We suspect that these images were generated from slow-growing organisms for which subunit production could keep pace with elongation or from cells imaged in the stationary phase when little to no growth occurs. To our knowledge, no freeze-fracture images with this level of resolution exist for *B. anthracis*, likely because of its pathogenic potential. However, we note that gaps in the *B. anthracis* S-layer have been previously observed with partially functional fluorescent protein fusions to Sap[29,41] and separately using electron microscopy[42]. Furthermore, recent studies on the *C. glutamicum* S-layer revealed incomplete S-layer coverage[26,43]. Accordingly, the incomplete encapsulation of the bacterium with an S-layer may be more common than previously appreciated and suggests that models in which the S-layer functions as a physical barrier to protect cells from external threats merit re-evaluation.

In conclusion, we have shown that the *B. anthracis* S-layer assembly during growth involves pervasive hoop-like cracks in the paracrystalline lattice. These cracks are formed by local pulling forces generated by expansion of the underlying PG. The incorporation of new Sap subunits to fill these cracks leads to both dispersed and focused S-layer assembly. We propose that dispersed assembly involves sealing the hoop-like cracks, whereas focused synthesis results from a failure to seal them, ensuring additional rounds of expansion and fill-in. This mechanism of S-layer expansion is likely to be broadly conserved among Gram-positive bacteria that elongate by dispersed cell wall synthesis.

Methods

Bacterial strains and media

All *B. anthracis* strains were derived from BaR1, the plasmid-free non-pathogenic Sterne derivative *B. anthracis* 9131 (ref. 44). *B. anthracis* cells were cultured in brain heart infusion (BHI) broth or agar at 37 °C unless indicated otherwise. When required, BHI medium was supplemented with chloramphenicol (5 μg ml^{-1}), erythromycin (5 μg ml^{-1}), kanamycin (25 μg ml^{-1}) or spectinomycin (300 μg ml^{-1}). IPTG was used at 0.5 mM.

Strain and plasmid construction

Deletions, point mutations and integration of transgenes at neutral chromosomal loci were generated by allelic exchange using pMiniMAD3 or pFR50, both derived from pMAD[45]. The plasmids were prepared in *Escherichia coli* strain SC110 and electroporated into *B. anthracis* followed by selection on BHI agar supplemented with spectinomycin or erythromycin as described previously[46]. A colony was then grown in 5 ml BHI-spec or BHI-erm at 30 °C. After 10 h of growth, the culture was serially diluted, plated on BHI-spec or BHI-erm plates and incubated overnight at 42 °C to select for cells with a single crossover integration (loop-in). A single colony was then grown without selection in 5 ml BHI at 30 °C for 24 h. The culture was serially diluted and plated on BHI agar or BHI supplemented with the second antibiotic. Plates were incubated overnight at 37 °C. Colonies were screened for loop-out by sensitivity to spectinomycin or erythromycin. Allelic exchange was confirmed using PCR. Tables of strains (Supplementary Table 1), plasmids (Supplementary Table 2) and oligonucleotide primers (Supplementary Table 3) and a description of plasmid constructions can be found in Supplementary Information.

Growth conditions and labelling

B. anthracis strains were cultured identically for all experiments in this study. In brief, a freshly streaked colony from a BHI agar plate was used to inoculate 3 ml BHI medium. The cells were grown within a roller drum at 37 °C for 2 h. This exponentially growing preculture was used to inoculate BHI medium at an OD_{600} of 0.02 and grown at 37 °C to an OD_{600} of ~0.15. The cells were then labelled with maleimide-conjugated dyes or anti-ALFA nanobodies as described below and imaged or returned to fresh medium for pulse-chase experiments.

For maleimide-conjugated dyes, 2 ml of cells expressing Sap^{cys} at OD_{600} of ~0.15 was pelleted, washed once with PBS and incubated in 0.5 ml PBS with 10 μM maleimide-STAR RED (Abberior), STAR GREEN (Abberior) or CF594 (Biotium) for 10 min at room temperature in the dark. For ALFA-tag labelling, cells expressing Sap^{ALFA} were collected, washed identically and then incubated in 0.5 ml PBS with 25 nM anti-AFLA-ATTO488 (Nanotag) for 10 min in the dark. After labelling, cells were washed once with PBS to remove unincorporated dye or unbound nanobodies, concentrated and spotted on a 1% PBS agarose pad for imaging. For pulse-chase experiments, the cells were inoculated

in BHI at an OD_{600} of 0.1. At time points during growth, cells were collected and imaged, or labelled and then imaged as described above. For time-lapse microscopy, 5 μg ml^{-1} FM4-64 was included in the BHI agarose pad to visualize cell membranes. For imaging the cell wall PG, ATTO488-D-lys-NH_2 (15 nM), HADA (100 μM) or NADA (100 μM) was added to the cell culture for 1–2 h before collection.

For analysis of the S-layer following fosfomycin treatment, early-exponential *sap*^{cys} cells (OD_{600} ~ 0.1) were incubated in BHI with fosfomycin (350 μg ml^{-1}) for 45 min, then labelled with STAR RED in PBS and returned to fresh BHI medium in the presence of fosfomycin. Cells were visualized after 0 min, 15 min and 30 min. Shorter incubation times with fosfomycin before Sap^{cys} labelling did not fully stop growth during the chase; increasing the concentration of fosfomycin caused excessive lysis during the chase.

Light microscopy

Widefield microscopy of live cells was performed at 30 °C using a Nikon Ti2-E inverted microscope (100× oil objective, numerical aperture (NA) 1.45). For snapshots, 50% illumination power and 100 ms exposure were used for fluorescent channels. For time-lapse imaging, cells were placed on BHI agarose pads for 30 min at room temperature before imaging. For image acquisition, 10% illumination power and 100 ms exposure were used. The phase-contrast images were acquired with 100 ms exposure using 98% transmitted light.

Three-dimensional confocal microscopy was performed at room temperature using a Leica Stellaris 8 Falcon microscope (63× oil objective, NA 1.4). Cells were collected and immediately fixed in 2.6% formaldehyde and 0.04% glutaraldehyde in PBS for 30 min before imaging. The highest possible resolution was applied under 'Lightning' mode using 2% of the laser power, a gain of 10 and a zoom factor of 3 for image acquisition. The focal plane was adjusted manually, and then a total range of 3 μm depth was applied to acquire the full image stack with 136 nm between slices. The final pixel size was 35.54 nm. The 3D reconstruction was generated in ImageJ.

STED microscopy was performed at room temperature using an Abberior STEDYCON microscope mounted on a Nikon N-SIM (100× oil objective, NA 1.4). Cells were collected and fixed as described above. A small region of interest containing 1–3 bacteria was chosen for imaging. Fluorescence was collected through a 1.1 Airy unit pinhole@650 nm. Confocal images were first acquired using no depletion laser, an average pixel dwell time of 10 μs $pixel^{-1}$ and 2-line accumulations. An excitation power of 10 (CF594) or 0.2% (STAR RED) was used. STED images had an average pixel dwell time of 50 μs $pixel^{-1}$ and 5-line accumulations. A 100% (CF594) or 1% (STAR RED) excitation power was used. CF594 and STAR RED were spectrally filtered from 575 nm to 625 nm, and 650 nm to 700 nm, respectively, using a Si avalanche photodiode detector. Both confocal and STED images had a pixel size of 25 nm.

Fluorescence recovery after photobleaching experiments were performed at room temperature using a Zeiss LSM 980 confocal microscope (100× oil objective, NA 1.4). The P_{IPTG}-*sap*^{cys} Δ*sap* Δ*eag* strain was grown in BHI supplemented with 0.5 mM IPTG for 1.5 h (final OD_{600} ~ 0.25), followed by dye labelling and mounting on a 1% BHI agarose pad supplemented with 0.5 mM IPTG. Manually selected regions along the cell cylinder (~500 nm sized spot) were bleached (pixel dwell time ~7 μs) using 100% laser power at 639 nm. Images before and after bleaching were acquired using 2% laser power and a 0.38 s frame rate. Fluorescence recovery was monitored for ~90 s post-bleaching.

Electron microscopy

Transmission electron microscopy was performed using a JEOL 1200EX microscope. A 500 μl volume of bacterial cell culture was collected and immediately mixed with 500 μl of 2× electron microscopy fixative solution containing 2.5% formaldehyde, 1.25% glutaraldehyde and 0.06% picric acid in 0.1 M sodium cacodylate buffer (pH 7.4) in a 1.7 ml microfuge tube, followed by centrifugation to fix cells as pellets. The pelleted cells and supernatant were incubated overnight at 4 °C. Samples were then washed 3× with cacodylate buffer and incubated with 1% osmium tetroxide and 1.5% potassium ferrocyanide for 1 h. After washing 3× with water, samples were stained with 1% uranyl acetate in water for 1 h and then washed 3× with water. Samples were dehydrated with an increasing gradient of ethanol solutions (50%, 75%, 95% and 100%) for 15 min each, followed by incubation with propylene oxide for 1 h, and embedded in Epon that was mixed 1:1 with propylene oxide. Samples were allowed to polymerize at 60 °C for 48 h and sectioned to a thickness of 50–60 nm before imaging.

Sap fractionation and in-gel fluorescence and Coomassie staining

Surface-associated and released Sap^{cys} proteins were extracted or collected, concentrated and analysed as follows. Cells expressing Sap^{cys} were labelled using maleimide-STAR RED as described above and inoculated into BHI medium. At the indicated times, an equal volume of culture (1 ml) was removed, and the cells were pelleted via centrifugation. A 900 μl volume of the culture medium was removed, mixed with 100 μl of 100% TCA (10% final) and placed on ice. The rest of the supernatant was carefully removed, and the cell pellet was resuspended in 1 ml of 3 M urea in PBS and incubated at 95 °C for 10 min to extract the surface-associated Sap^{cys} protein. The mixture was then centrifuged (16,000*g*, 10 min), and 900 μl of supernatant was removed, mixed with 100 μl of 100% TCA and placed on ice. After 30 min incubation on ice, the TCA-precipitated Sap^{cys} from the culture medium and extracted from the cell surface was collected via centrifugation (16,000*g*, 10 min). The pellets were washed once with ice-cold acetone and then resuspended in 100 μl of 0.5 M Tris-HCl (pH 8.0) with 4% sodium dodecyl sulfate (SDS). A 10 μl volume of the TCA-precipitated material was mixed with an equal volume of 2× Laemmli SDS sample buffer containing 10% β-mercaptoethanol and resolved via SDS–polyacrylamide gel electrophoresis using a 4–20% polyacrylamide Mini-PROTEAN TGX gel (Bio-Rad). The gel was visualized on a Bio-Rad ChemiDoc using 647 nm ex. and then stained with InstantBlue (Abcam). The InstantBlue staining serves as a loading control, documenting the increase in total labelled + unlabelled Sap^{cys} during the cold chase.

To monitor Sap^{cys} proteins in the context of the native S-layer (Fig. 2e), 10 ml of cells (OD_{600} ~ 0.15) was labelled with STAR RED and resuspended in 10 ml fresh BHI medium. Every 15 min, 1 ml of culture was collected and fractionated. To determine whether Sap^{cys} expressed in the absence of the native S-layer gets shed (Extended Data Fig. 7a), 2 ml of cell culture after 2 h IPTG induction (OD_{600} ~ 0.6) was collected and fractionated.

Statistics and reproducibility

Microscopy images shown in Figs. 1c,d,f; 3a,b; 4a,c,d; and Extended Data Figs. 2b–d; 3a–d; 4a,b; 5a–c; 6a; 7a; 8a are representative of experiments from two or more biological replicates.

Reporting summary

Further information on research design is available in the Nature Portfolio Reporting Summary linked to this article.

Data availability

No large-scale datasets were generated in this study. All relevant data are available in the supplementary material. Raw data for all graphs and uncropped gel images have been uploaded as source data. Primers, synthetic DNA constructs and strains used can be found in supplementary tables. Source data are provided with this paper.

References

1. Sleytr, U. B., Schuster, B., Egelseer, E.-M. & Pum, D. S-layers: principles and applications. *FEMS Microbiol. Rev.* **38**, 823–864 (2014).

2. Isbilir, B., von Kügelgen, A., Alva, V. & Bharat, T. A. M. Assembly, architecture and functional roles of microbial surface layers. *Nat. Rev. Microbiol.* **24**, 344–358 https://doi.org/10.1038/s41579-025-01258-8 (2026).
3. Rothfuss, H., Lara, J. C., Schmid, A. K. & Lidstrom, M. E. Involvement of the S-layer proteins Hpi and SlpA in the maintenance of cell envelope integrity in *Deinococcus radiodurans* R1. *Microbiology* **152**, 2779–2787 (2006).
4. Zhang, C. et al. Cell structure changes in the hyperthermophilic crenarchaeon *Sulfolobus islandicus* lacking the S-layer. *mBio* **10**, e01589-19 https://doi.org/10.1128/mbio.01589-19 (2019).
5. Fioravanti, A., Mathelie-Guinlet, M., Dufrêne, Y. F. & Remaut, H. The *Bacillus anthracis* S-layer is an exoskeleton-like structure that imparts mechanical and osmotic stabilization to the cell wall. *PNAS Nexus* **1**, pgac121 (2022).
6. Fioravanti, A. et al. Structure of S-layer protein Sap reveals a mechanism for therapeutic intervention in anthrax. *Nat. Microbiol.* **4**, 1805–1814 (2019).
7. Sogues, A. et al. Structure and function of the EA1 surface layer of *Bacillus anthracis*. *Nat. Commun.* **14**, 7051 (2023).
8. Merrigan, M. M. et al. Surface-layer protein A (SlpA) is a major contributor to host-cell adherence of *Clostridium difficile*. *PLoS ONE* **8**, e78404 (2013).
9. Ali, S. et al. Slr4, a newly identified S-layer protein from marine Gammaproteobacteria, is a major biofilm matrix component. *Mol. Microbiol.* **114**, 979–990 (2020).
10. Kirk, J. A. et al. New class of precision antimicrobials redefines role of *Clostridium difficile* S-layer in virulence and viability. *Sci. Transl. Med.* **9**, eaah6813 (2017).
11. Rados, T. et al. Tissue-like multicellular development triggered by mechanical compression in archaea. *Science* **388**, 109–115 (2025).
12. Kern, J. W. & Schneewind, O. BslA, a pXO1-encoded adhesin of *Bacillus anthracis*. *Mol. Microbiol.* **68**, 504–515 (2008).
13. Wang, Y. et al. *Bacillus anthracis* S-layer protein BslA binds to extracellular matrix by interacting with laminin. *BMC Microbiol.* **16**, 183 (2016).
14. Uchida, M. et al. Protective effect of *Bacillus anthracis* surface protein EA1 against anthrax in mice. *Biochem. Biophys. Res. Commun.* **421**, 323–328 (2012).
15. Bharat, T. A. M., von Kügelgen, A. & Alva, V. Molecular logic of prokaryotic surface layer structures. *Trends Microbiol.* **29**, 405–415 (2021).
16. Lanzoni-Mangutchi, P. et al. Structure and assembly of the S-layer in *C. difficile*. *Nat. Commun.* **13**, 970 (2022).
17. Sivabalasarma, S., van Wolferen, M., Albers, S.-V. & Charles-Orszag, A. Biogenesis, function and evolution of the archaeal S-layer. *Curr. Opin. Cell Biol.* **95**, 102534 (2025).
18. Awram, P. & Smit, J. Identification of lipopolysaccharide O antigen synthesis genes required for attachment of the S-layer of *Caulobacter crescentus*. *Microbiology* **147**, 1451–1460 (2001).
19. von Kügelgen, A. et al. In situ structure of an intact lipopolysaccharide-bound bacterial surface layer. *Cell* **180**, 348–358.e15 (2020).
20. Sagmeister, T. et al. The molecular architecture of *Lactobacillus* S-layer: assembly and attachment to teichoic acids. *Proc. Natl Acad. Sci.* **121**, e2401686121 (2024).
21. Bönisch, E. et al. Lipoteichoic acid mediates binding of a *Lactobacillus* S-layer protein. *Glycobiology* **28**, 148–158 (2018).
22. Sychantha, D. et al. Molecular basis for the attachment of S-layer proteins to the cell wall of *Bacillus anthracis*. *Biochemistry* **57**, 1949–1953 (2018).
23. Chapman, R. N., Liu, L. & Boons, G.-J. 4,6-*O*-Pyruvyl ketal modified *N*-acetylmannosamine of the secondary cell wall polysaccharide of *Bacillus anthracis* is the anchoring residue for its surface layer proteins. *J. Am. Chem. Soc.* **140**, 17079–17085 (2018).
24. Comerci, C. J. et al. Topologically-guided continuous protein crystallization controls bacterial surface layer self-assembly. *Nat. Commun.* **10**, 2731 (2019).
25. Herdman, M. et al. Cell cycle dependent coordination of surface layer biogenesis in *Caulobacter crescentus*. *Nat. Commun.* **15**, 3355 (2024).
26. Sogues, A. et al. Cryo-EM structure and polar assembly of the PS2 S-layer of *Corynebacterium glutamicum*. *Proc. Natl Acad. Sci.* **122**, e2426928122 (2025).
27. Oatley, P., Kirk, J. A., Ma, S., Jones, S. & Fagan, R. P. Spatial organization of *Clostridium difficile* S-layer biogenesis. *Sci. Rep.* **10**, 14089 (2020).
28. Harrison, G. A. & Shen, A. Molecular dissection of class A PBP function uncovers novel features of the non-canonical *Clostridioides difficile* divisome complex. *PLoS Genet* **21**, e1011746 (2025).
29. Kern, V. J., Kern, J. W., Theriot, J. A., Schneewind, O. & Missiakas, D. Surface-layer (S-layer) proteins Sap and EA1 govern the binding of the S-layer-associated protein BslO at the cell septa of *Bacillus anthracis*. *J. Bacteriol.* **194**, 3833–3840 (2012).
30. Mignot, T., Mesnage, S., Couture-Tosi, E., Mock, M. & Fouet, A. Developmental switch of S-layer protein synthesis in *Bacillus anthracis*. *Mol. Microbiol.* **43**, 1615–1627 (2002).
31. Sogues, A. et al. Architecture of the Sap S-layer of *Bacillus anthracis* revealed by integrative structural biology. *Proc. Natl Acad. Sci.* **121**, e2415351121 (2024).
32. Götzke, H. et al. The ALFA-tag is a highly versatile tool for nanobody-based bioscience applications. *Nat. Commun.* **10**, 4403 (2019).
33. Kuru, E. et al. In situ probing of newly synthesized peptidoglycan in live bacteria with fluorescent D-amino acids. *Angew. Chem. Int. Ed.* **51**, 12519–12523 (2012).
34. Rohs, P. D. A. & Bernhardt, T. G. Growth and division of the peptidoglycan matrix. *Annu. Rev. Microbiol.* **75**, 315–336 (2021).
35. Doyle, R. J., Chaloupka, J. & Vinter, V. Turnover of cell walls in microorganisms. *Microbiol. Rev.* **52**, 554–567 (1988).
36. Reith, J. & Mayer, C. Peptidoglycan turnover and recycling in Gram-positive bacteria. *Appl. Microbiol. Biotechnol.* **92**, 1–11 (2011).
37. Erickson, H. P. How teichoic acids could support a periplasm in Gram-positive bacteria, and let cell division cheat turgor pressure. *Front. Microbiol.* **12**, 664704 (2021).
38. Remsen, C. C., Watson, S. W., Waterbury, J. B. & Trüper, H. G. Fine structure of *Ectothiorhodospira mobilis* Pelsh. *J. Bacteriol.* **95**, 2374–2392 (1968).
39. Sleytr, U., Adam, H. & Klaushofer, H. Die Feinstruktur der Zellwand und Cytoplasmamembran von *Clostridium nigrificans*, dargestellt mit Hilfe der Gefrierätz- und Ultradünnschnittechnik. *Arch. Mikrobiol.* **66**, 40–58 (1969).
40. Sleytr, U. B. & Pum, D. S-layers: from a serendipitous discovery to a toolkit for nanobiotechnology. *Q. Rev. Biophys.* **58**, e4 (2025).
41. Anderson, V. J., Kern, J. W., McCool, J. W., Schneewind, O. & Missiakas, D. The SLH-domain protein BslO is a determinant of *Bacillus anthracis*chain length. *Mol. Microbiol.* **81**, 192–205 (2011).
42. Couture-Tosi, E. et al. Structural analysis and evidence for dynamic emergence of *Bacillus anthracis* S-layer networks. *J. Bacteriol.* **184**, 6448–6456 (2002).
43. Isbilir, B., Yeates, A., Alva, V. & Bharat, T. A. M. Mapping the ultrastructural topology of the corynebacterial cell surface. *PLoS Biol.* **23**, e3003130 (2025).
44. Etienne-Toumelin, I., Sirard, J. C., Duflot, E., Mock, M. & Fouet, A. Characterization of the *Bacillus anthracis* S-layer: cloning and sequencing of the structural gene. *J. Bacteriol.* **177**, 614–620 (1995).

45. Arnaud, M., Chastanet, A. & Débarbouillé, M. New vector for efficient allelic replacement in naturally nontransformable, low-GC-content, Gram-positive bacteria. *Appl. Environ. Microbiol.* **70**, 6887–6891 (2004).
46. Ramírez-Guadiana, F. H. et al. Identification of sporulation genes in *Bacillus anthracis* highlights similarities and significant differences with *Bacillus subtilis*. *PLoS Biol.* **23**, e3003521 (2025).

Acknowledgements

We thank all the members of the Bernhardt-Rudner supergroup for helpful advice, discussions and encouragement; F. Ramírez-Guadiana for advice and training; the HMS MicRoN Core for support and assistance; the HMS Electron Microscopy Facility for consultation and services; D. Kearns (Indiana University) for pMiniMAD vectors; E. Garner (Harvard University) for ATTO488-D-lys-NH_2; and J. Kirby (Beth Israel Deaconess Medical Center) for sharing strains.

Author contributions

C.Z. and D.Z.R. conceptualized the project. C.Z. and Y.Y. performed the experiments. C.Z. and Q.Y. performed the analyses. D.Z.R. supervised the study. C.Z. and D.Z.R. wrote the original draft. All authors reviewed and edited the paper.

Funding

Support for this work comes from the National Institutes of Health grant numbers R01AI164647, R21AI171308 and R35GM145299 (D.Z.R.). C.Z. was funded in part by an HFSP Long-term Postdoctoral Fellowship (LT0001/2025-L), and Q.Y. was supported in part by a Harold W. Dodds Fellowship from Princeton University.

Competing interests

The authors declare no competing interests.

Additional information

Extended data is available for this paper at https://doi.org/10.1038/s41564-026-02544-8.

Supplementary information The online version contains supplementary material available at https://doi.org/10.1038/s41564-026-02544-8.

Correspondence and requests for materials should be addressed to David Z. Rudner.

Peer review information *Nature Microbiology* thanks Tanmay Bharat, Robert Fagan and the other, anonymous, reviewer(s) for their contribution to the peer review of this work. Peer reviewer reports are available.

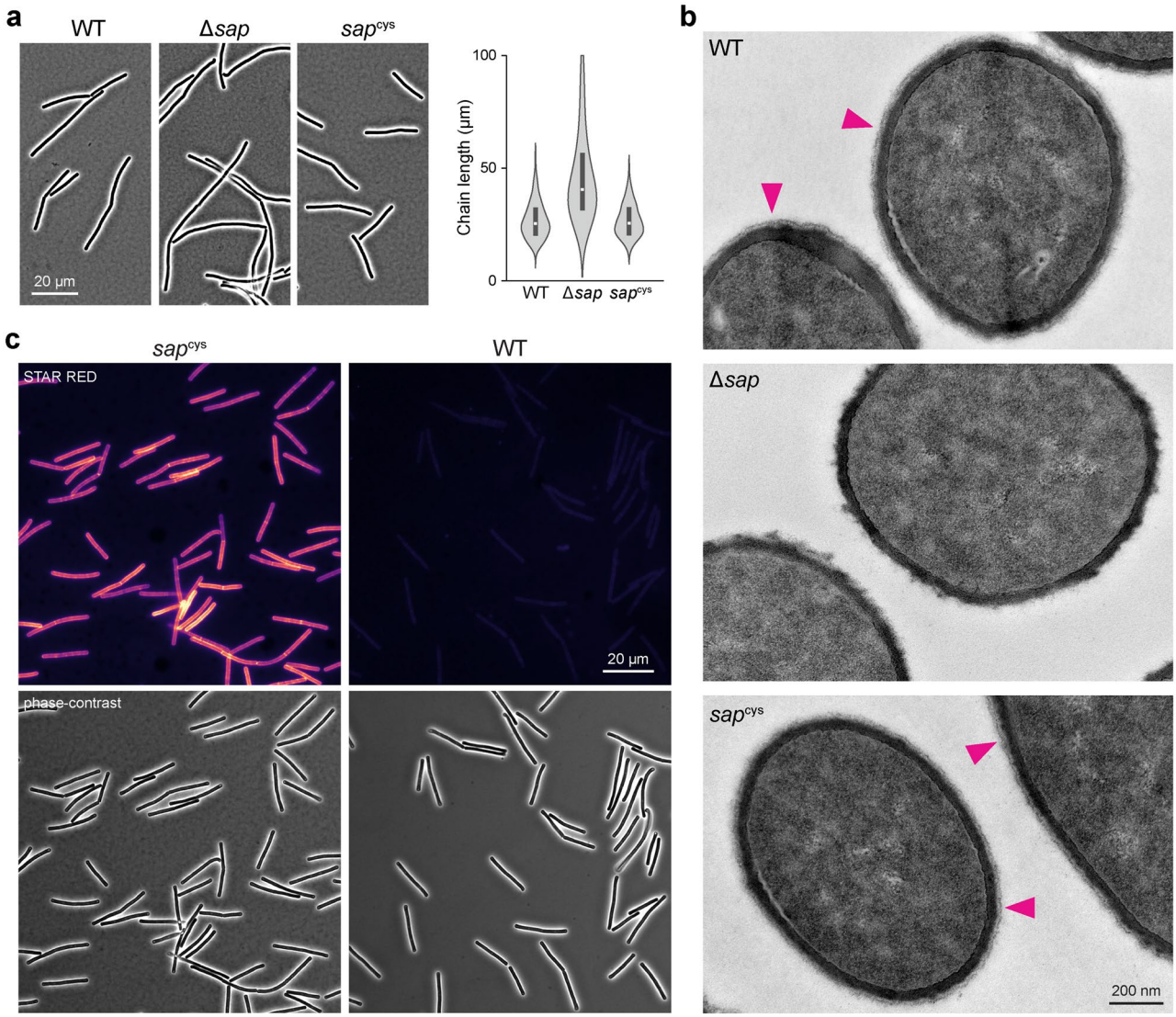
Reprints and permissions information is available at www.nature.com/reprints.

Publisher's note Springer Nature remains neutral with regard to jurisdictional claims in published maps and institutional affiliations.

Open Access This article is licensed under a Creative Commons Attribution-NonCommercial-NoDerivatives 4.0 International License, which permits any non-commercial use, sharing, distribution and reproduction in any medium or format, as long as you give appropriate credit to the original author(s) and the source, provide a link to the Creative Commons licence, and indicate if you modified the licensed material. You do not have permission under this licence to share adapted material derived from this article or parts of it. The images or other third party material in this article are included in the article's Creative Commons licence, unless indicated otherwise in a credit line to the material. If material is not included in the article's Creative Commons licence and your intended use is not permitted by statutory regulation or exceeds the permitted use, you will need to obtain permission directly from the copyright holder. To view a copy of this licence, visit http://creativecommons.org/licenses/by-nc-nd/4.0/.

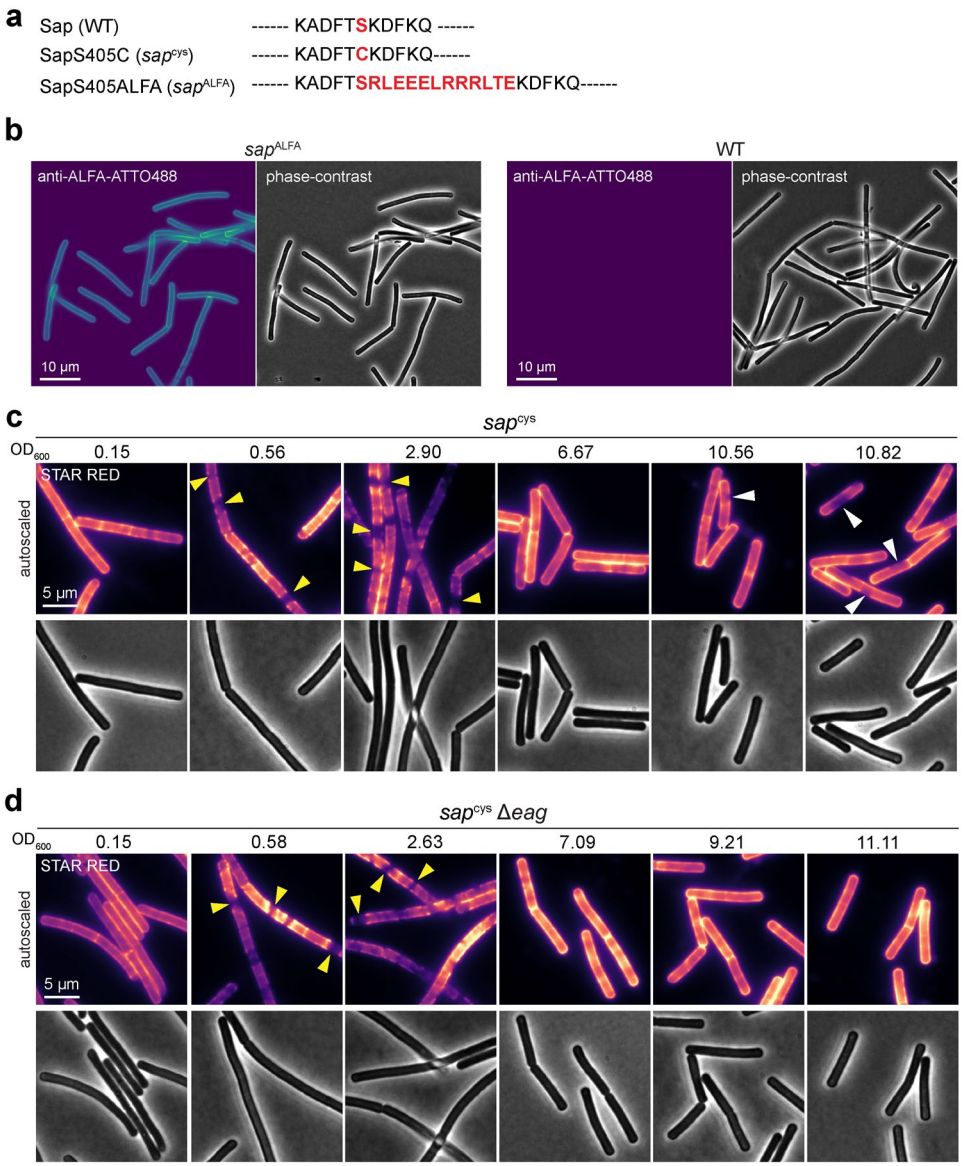
© The Author(s) 2026

https://doi.org/10.1038/s41564-026-02544-8



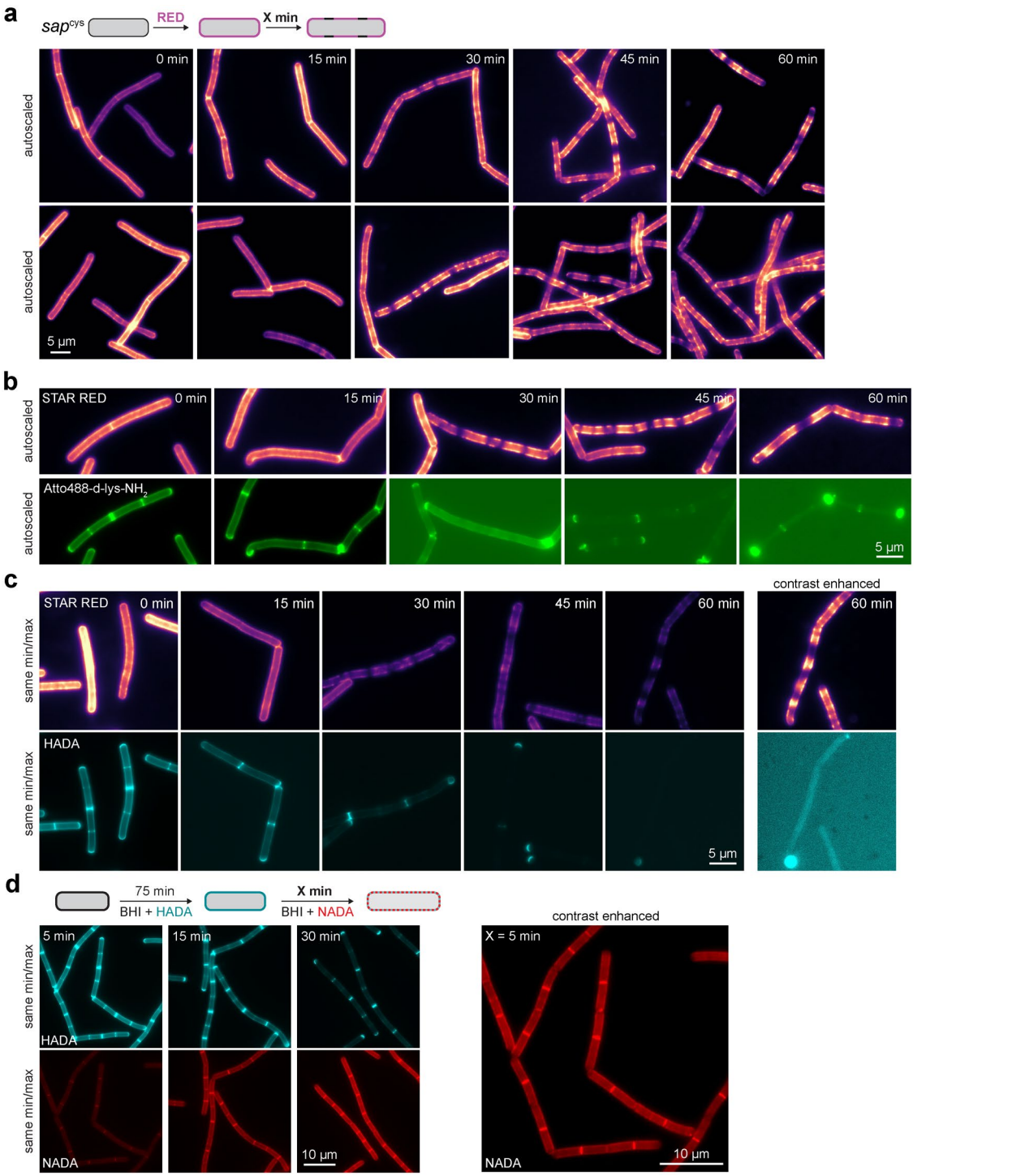
Extended Data Fig. 1 | Visualizing the *B. anthracis* Sap S-layer. (**a**) The *sap*^{cys} allele is functional. Representative phase-contrast images of the indicated strains (left). Chain length distributions of the WT (n = 410), Δ*sap* (n = 203), and *sap*^{cys} strains (n = 146) (right). Data are presented as violin plots with median (centre white circle) and interquartile range (25th to 75th percentile, bounds of the gray boxes) indicated. Data are from 3 biological replicates. (**b**) Representative transmission electron micrographs of the indicated strains. The S-layer (pink carets) is indicated. (**c**) Representative fluorescence and phase-contrast images of the indicated strains. Early exponential phase cells were labelled with maleimide-STAR RED and imaged. The fluorescence images were processed identically with the same min/max intensities applied.

https://doi.org/10.1038/s41564-026-02544-8



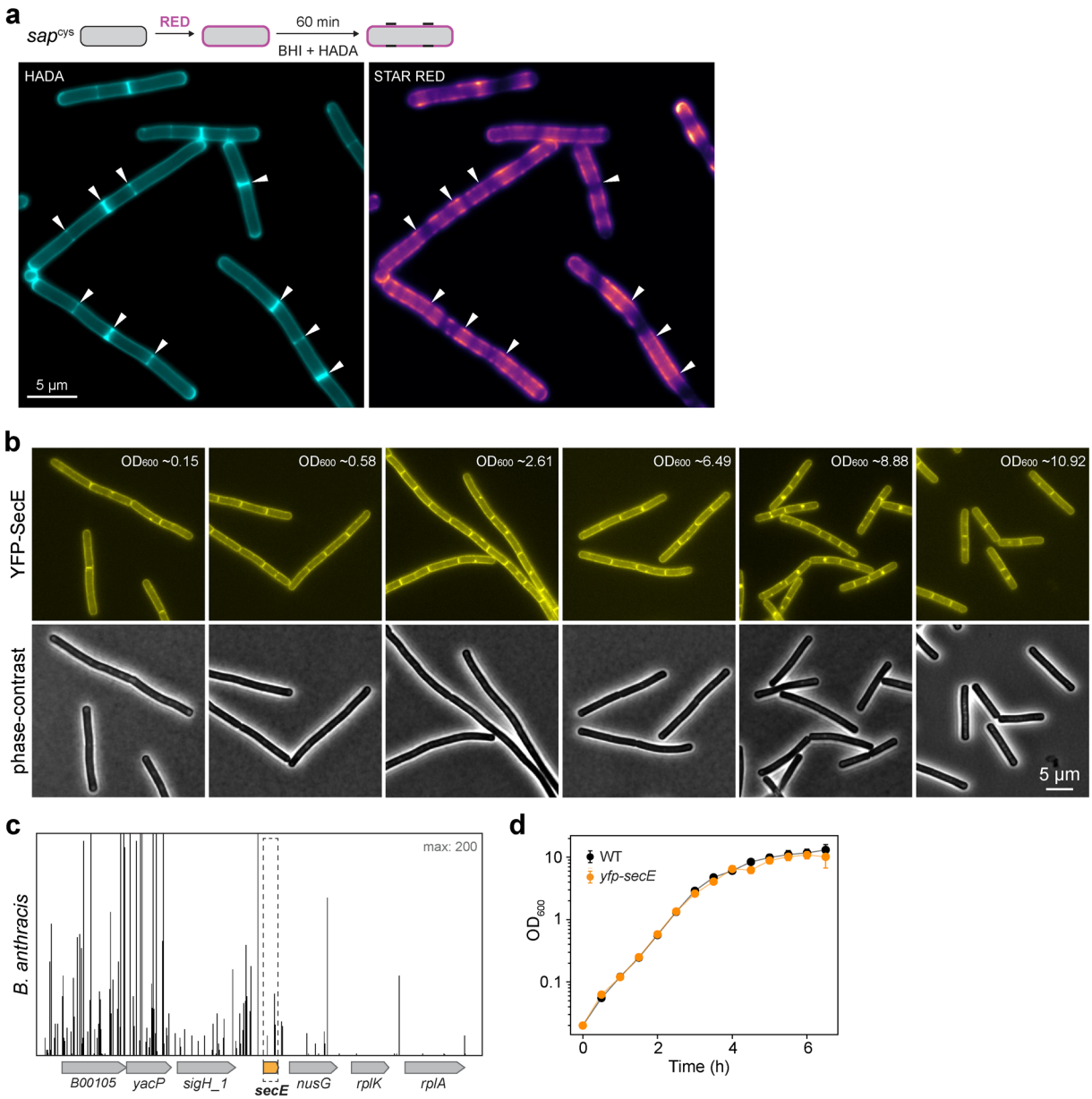
Extended Data Fig. 2 | Dark patches in the Sap S-layer in stationary phase are lost in the absence of *eag*. (**a**) Diagram of amino acid substitutions at S405 in Sap. Serine-405 was replaced with cysteine in *sap*^{cys} and with the ALFA tag in *sap*^{ALFA}. (**b**) Representative immunofluorescence and phase-contrast images of WT and *sap*^{ALFA} cells. Early exponential phase cells (OD_{600} ~ 0.15) were labelled with anti-ALFA-ATTO488 nanobodies. The fluorescence images were processed identically with the same min/max intensities applied. (**c**,**d**) Representative fluorescence and phase-contrast images of *sap*^{cys} and *sap*^{cys} Δ*eag* throughout growth. Dark bands in mid- and late-exponential growth phases (yellow carets) and dark patches in stationary phase (white carets) are highlighted. The fluorescence images in (**c**) and (**d**) were autoscaled.

https://doi.org/10.1038/s41564-026-02544-8



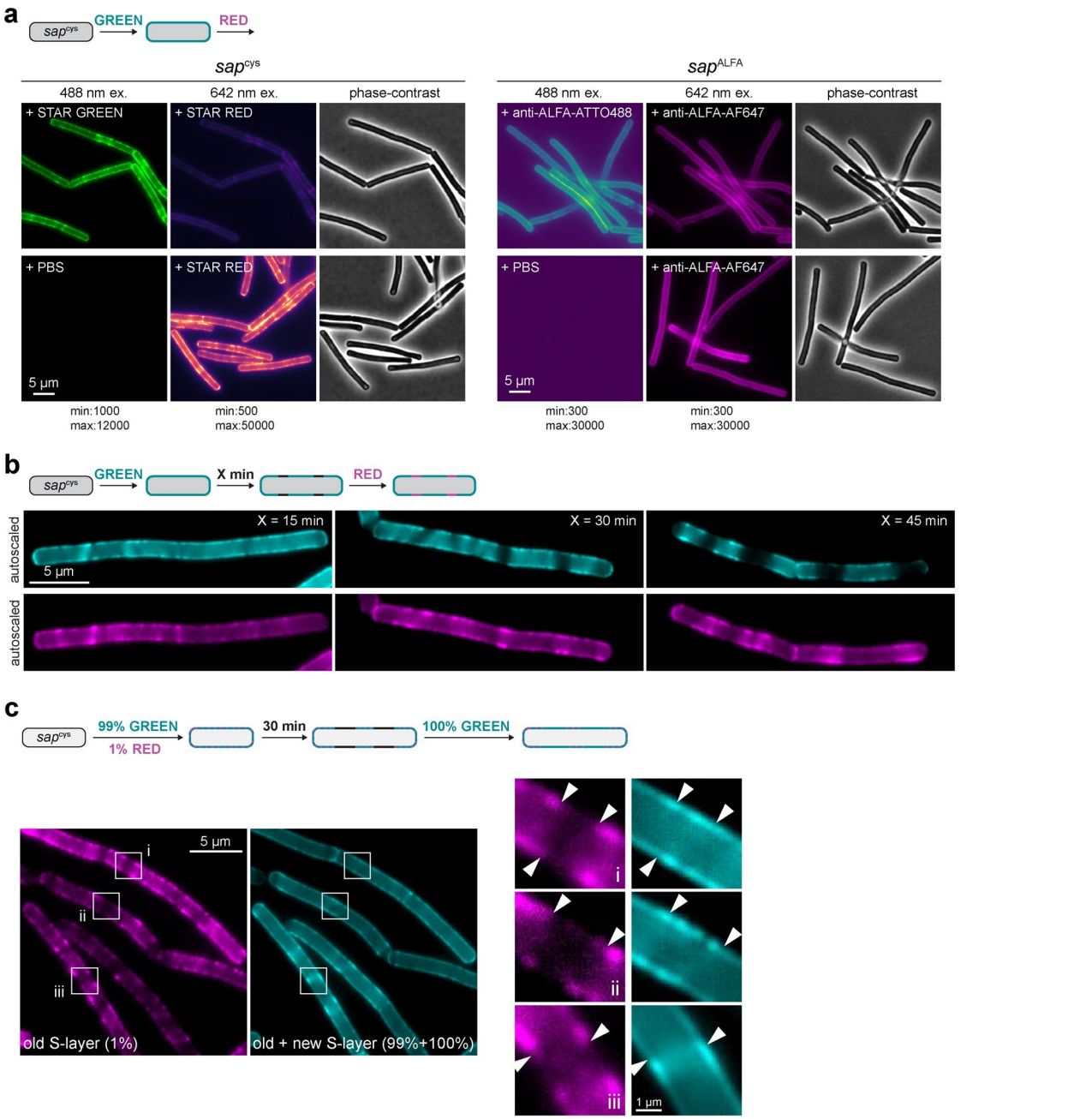
Extended Data Fig. 3 | Focused S-layer assembly is not due to focused cell wall assembly. (**a**) Schematic of the cold-chase assay (top). *sap*^{cys} cells were labelled with STAR RED and returned to growth medium and imaged at timepoints after. Representative fluorescence images of the S-layer at the indicated times after the return to growth (bottom). Images were autoscaled to highlight the dark bands of newly synthesized unlabelled Sap^{cys}. (**b**) The cell wall PG was labelled with the FDAA ATTO488-D-lysine-NH_2 for 2 h prior to pulse-labelling Sap^{cys}. The images shown are the same as in Fig. 2a, except that they are autoscaled to more clearly visualize the homogenous loss of FDAAs along the cell cylinder. (**c**) The cell wall PG was labelled with the FDAA HADA for 2 h prior to pulse-labelling Sap^{cys}. The fluorescence images were processed identically with the same min/max intensities applied. Contrast-enhanced images from 60 min after chase are shown to visualize the homogeneous loss of FDAAs along the cell cylinder. (**d**) Schematic of the pulse-chase assay (top). WT cells were labelled during growth in BHI supplemented with 100 µM HADA, washed with PBS, then returned to fresh BHI supplemented with 100 µM NADA and imaged at timepoints after. Representative fluorescence images of labelled cells at the indicated times after the return to growth (left). The fluorescence images for each channel were processed identically with the same min/max intensities applied. Contrast-enhanced image of NADA labelling 5 min after chase was enlarged to more clearly visualize the homogeneous incorporation of NADA along the cell cylinder (right).

https://doi.org/10.1038/s41564-026-02544-8



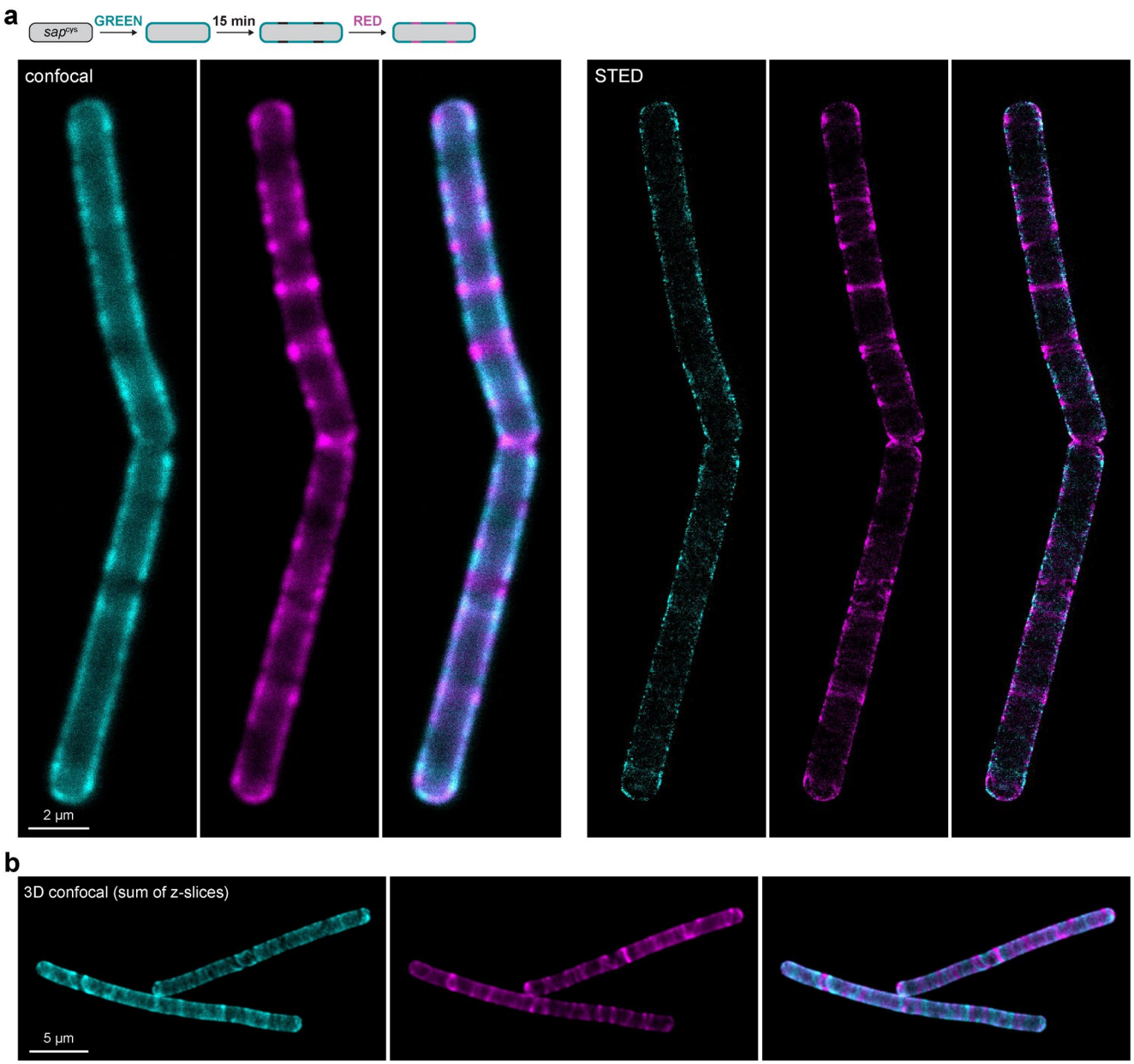
Extended Data Fig. 4 | Focused S-layer assembly does not co-localize with division sites nor can it be explained by the localization of Sec translocons. (**a**) Schematic of the cold-chase assay (top). *sap*^{cys} cells were labelled with STAR RED and returned to growth medium and imaged 60 min later. Representative fluorescence image of the S-layer (bottom). The cells were continuously labelled with HADA during the 60 min growth to visualize division septa, instead of the membrane dye FM4-64 used in Fig. 2b. Septa (white carets) are highlighted. (**b**) Representative fluorescence and phase-contrast images of a strain expressing a functional YFP-SecE fusion. (**c**) Transposon-insertion profile from a region of the *B. anthracis* genome that contains *secE*. The data are from a transposon-sequencing experiment reported in Ramirez-Gudiana et al. A deep transposon library was generated in *B. anthracis* and insertion sites and their abundance in the library were determined by deep sequencing and mapping to the reference genome. Each vertical line indicates a transposon insertion site. The height of the line reflects the number of sequencing reads at this position. The paucity of insertions in *secE* is consistent with the idea that SecE is essential for viability. (**d**) Growth curves of WT and *yfp-secE* fusion strains in rich medium. Data are means ± s.d. of 3 biological replicates.

https://doi.org/10.1038/s41564-026-02544-8



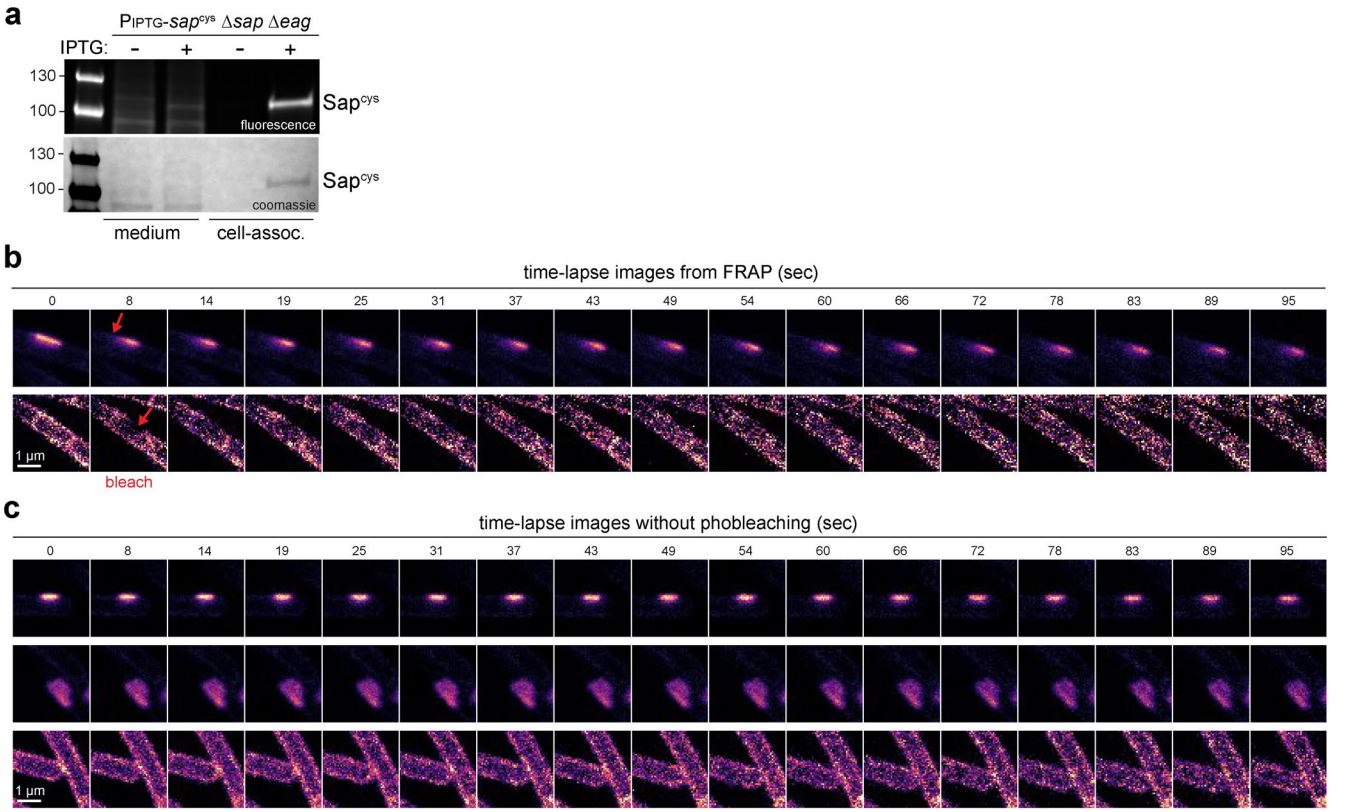
Extended Data Fig. 5 | New Sap is incorporated into the S-layer at the edge of the cracked lattice. (**a**) 10 µM maleimide-STAR GREEN labels virtually all free Sap^{cys} subunits in the S-layer. Schematic of the assay (top). Early exponential phase *sap*^{cys} cells were labelled with STAR GREEN (10 µM) or incubated with PBS, washed, and then immediately labelled with STAR RED. Representative fluorescence and phase-contrast images are shown (left panels). A similar experiment was performed in which early exponential phase *sap*^{ALFA} cells were incubated with anti-ALFA-ATTO488 (25 nM) or PBS, washed, and then immediately incubated with anti-ALFA-AF647. Representative fluorescence and phase-contrast images are shown (right panels). The min/max values used to scale the images for each color are indicated below. (**b**) Dual-color pulse-chase images in Fig. 3a we autoscaled to more easily visualize old and new Sap subunits in the S-layer lattice. (**c**) Schematic of the pulse-chase assay used to determine where newly synthesized Sap is incorporated into the S-layer lattice. Early exponentially growing *sap*^{cys} cells were pulse labelled with a mixture of STAR GREEN and STAR RED at a molar ratio of 99:1. The cells were returned to rich medium and grown for 30 min. The newly synthesized Sap^{cys} was then labelled with STAR GREEN. The trace amount of STAR RED-labelled Sap was used to monitor the old S-layer lattice and to identify dark bands that are sights of focused S-layer assembly. STAR GREEN fluorescence reports on both old and new S-layer and reveals continuous signal across the boundary. Three boxed regions are enlarged on the right. The junction between old and new S-layer are indicated with white carets.

https://doi.org/10.1038/s41564-026-02544-8



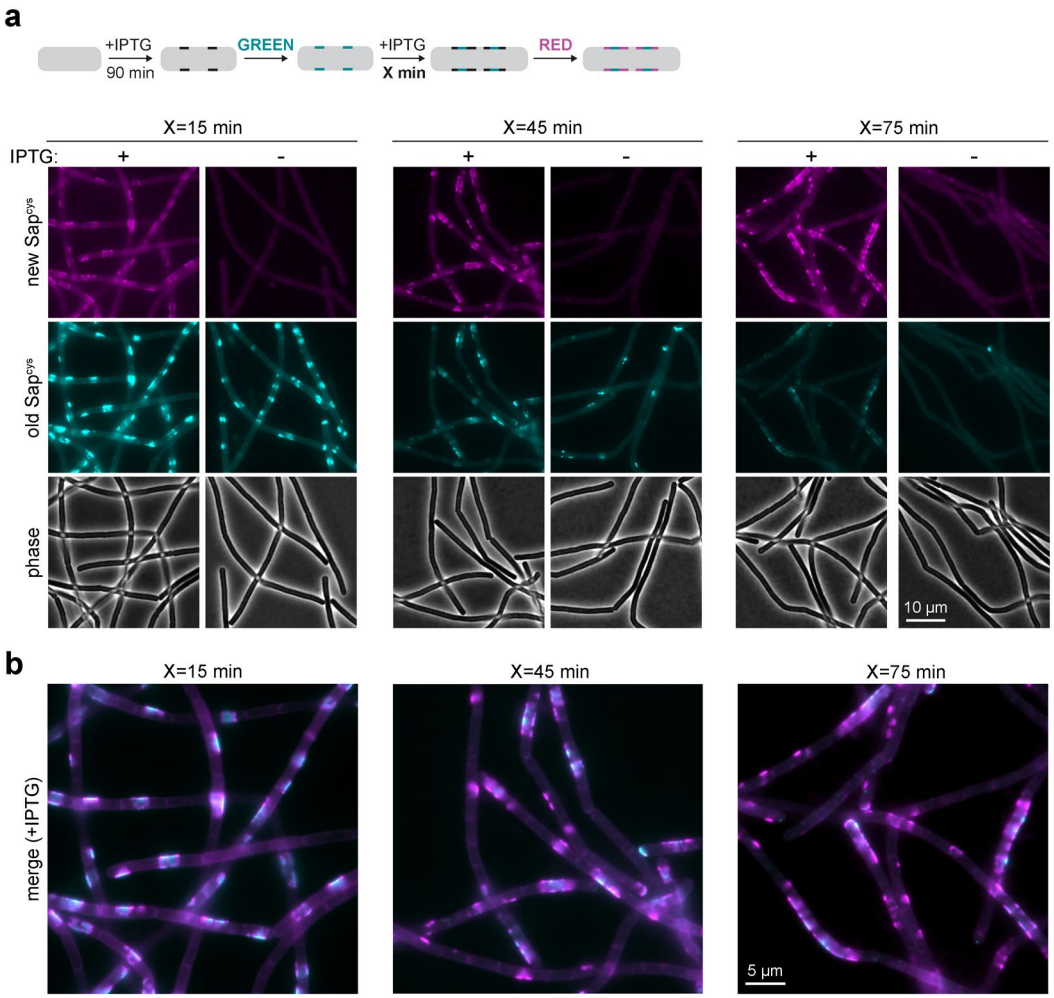
Extended Data Fig. 6 | STED and confocal images of S-layer assembly during growth. (**a**) Schematic of the dual-color pulse-chase imaging assay (top). Early exponentially growing cells were labelled with maleimide-CF594 then returned to growth medium for 15 min. The newly synthesized Sap^{cys} was labelled with STAR RED and the cells imaged by confocal (left) and STED (right) microscopy. The STED images are the same as those shown in Fig. 3b. (**b**) Early exponentially growing cells were labelled with maleimide-STAR GREEN then returned to growth medium for 15 min. The newly synthesized Sap^{cys} was labelled with STAR RED and the cells imaged by confocal microscopy. Sum of z-slices of 3D confocal images of old (left), new (middle), and merged (right) Sap^{cys} after the 15-min chase. The same field-of-view is shown in Fig. 3c.

https://doi.org/10.1038/s41564-026-02544-8



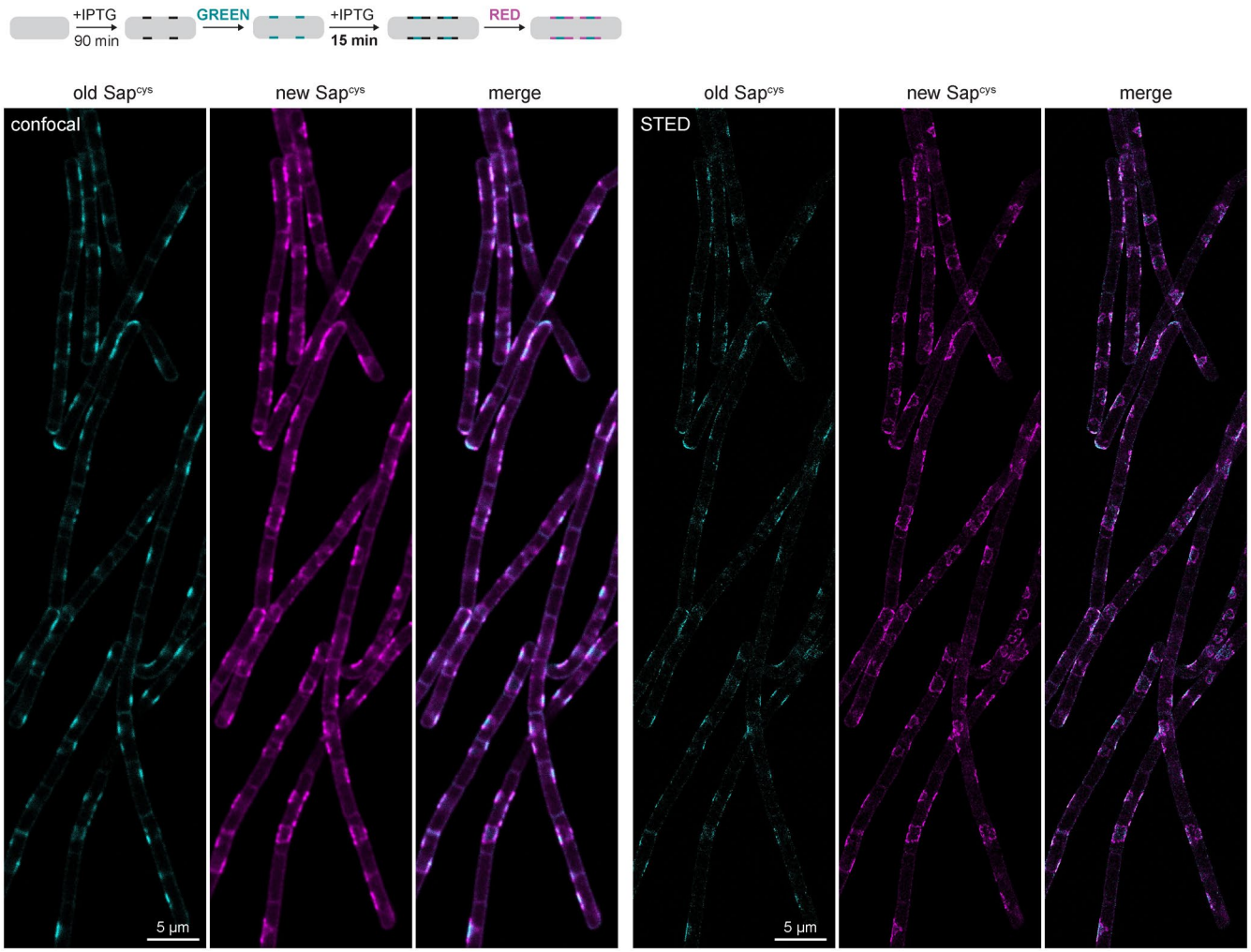
Extended Data Fig. 7 | Sap^{cys} expressed under IPTG control is not shed into the culture medium. (**a**) Representative in-gel fluorescence and Coomassie staining of Sap^{cys} protein present in the culture medium or extracted from the cell surface. The indicated strain was grown in rich medium with or without IPTG (0.5 mM) for 2 h, labelled with maleimide-STAR RED, and equivalent OD_{600} units were processed. Molecular weight markers in kDa are indicated. (**b**) Fluorescence images from a FRAP experiment in which a region containing a Sap-STAR RED raft was bleached (top) or a region on the cell surface lacking a raft was bleached (bottom). The images acquired directly after bleaching are indicated and a red arrow points to the bleached region. (**c**) Time-lapse fluorescence images acquired identically to the FRAP experiment in (b) but without photobleaching. Two regions containing a Sap-STAR RED raft and one region lacking a raft are shown.

https://doi.org/10.1038/s41564-026-02544-8



Extended Data Fig. 8 | De novo S-layer assembly dynamics revealed by dual-color pulse-chase. (**a**) Schematic of the dual-color pulse-chase assay (top). After 90 min of Sap^{cys} expression, the cells were labelled with STAR GREEN and then returned to rich medium with (or without) IPTG. At time points after, newly synthesized Sap^{cys} subunits were labelled with STAR RED and old and new S-layer material were visualized. Representative fluorescence and phase-contrast images at the indicate times after chase (bottom). The fluorescence images for each color were processed identically with the same min/max intensities applied. (**b**) Merged images of old and new Sap^{cys} at indicated times after chase. The images used in the merge are from panel a (+ IPTG).

https://doi.org/10.1038/s41564-026-02544-8



Extended Data Fig. 9 | Newly synthesized Sap^{cys} incorporates into the existing S-layer lattice. Schematic of the dual-color pulse-chase assay (top). After 90 min of Sap^{cys} expression, the cells were labelled with maleimide-CF594 and then returned to rich medium containing IPTG. 15 min later, newly synthesized Sap^{cys} subunits were labelled with STAR RED and old and new S-layer subunits were visualized. Representative confocal and STED images (bottom). These images come from the same field-of-view as shown in Fig. 4d.

nature portfolio

Corresponding author(s): David Z. Rudner

Last updated by author(s): Sep 25, 2026

Reporting Summary

Nature Portfolio wishes to improve the reproducibility of the work that we publish. This form provides structure for consistency and transparency in reporting. For further information on Nature Portfolio policies, see our Editorial Policies and the Editorial Policy Checklist.

Statistics

For all statistical analyses, confirm that the following items are present in the figure legend, table legend, main text, or Methods section.

n/a	Confirmed	
☐	☒	The exact sample size (*n*) for each experimental group/condition, given as a discrete number and unit of measurement
☐	☒	A statement on whether measurements were taken from distinct samples or whether the same sample was measured repeatedly
☒	☐	The statistical test(s) used AND whether they are one- or two-sided *Only common tests should be described solely by name; describe more complex techniques in the Methods section.*
☒	☐	A description of all covariates tested
☒	☐	A description of any assumptions or corrections, such as tests of normality and adjustment for multiple comparisons
☐	☒	A full description of the statistical parameters including central tendency (e.g. means) or other basic estimates (e.g. regression coefficient) AND variation (e.g. standard deviation) or associated estimates of uncertainty (e.g. confidence intervals)
☒	☐	For null hypothesis testing, the test statistic (e.g. *F*, *t*, *r*) with confidence intervals, effect sizes, degrees of freedom and *P* value noted *Give P values as exact values whenever suitable.*
☒	☐	For Bayesian analysis, information on the choice of priors and Markov chain Monte Carlo settings
☒	☐	For hierarchical and complex designs, identification of the appropriate level for tests and full reporting of outcomes
☒	☐	Estimates of effect sizes (e.g. Cohen's *d*, Pearson's *r*), indicating how they were calculated

Our web collection on statistics for biologists contains articles on many of the points above.

Software and code

Policy information about availability of computer code

Data collection	Wide-field microscopy data collection was performed using Nikon Elements (version 5.42.07) acquisition software. 3D confocal microscopy data collection was performed using Leica LasX (version 4.8.2.29567) acquisition software. STED microscopy data collection was performed using Abberior STEDYCON (serial SY241901) acquisition software. FRAP microscopy data collection was performed using Zeiss Zen Blue (version 3.7.97.09000) acquisition software.
Data analysis	Microscopy data analysis was performed using ImageJ (version 2.16.0/1.54p) software.

For manuscripts utilizing custom algorithms or software that are central to the research but not yet described in published literature, software must be made available to editors and reviewers. We strongly encourage code deposition in a community repository (e.g. GitHub). See the Nature Portfolio guidelines for submitting code & software for further information.

Data

Policy information about availability of data

All manuscripts must include a data availability statement. This statement should provide the following information, where applicable:

- Accession codes, unique identifiers, or web links for publicly available datasets
- A description of any restrictions on data availability
- For clinical datasets or third party data, please ensure that the statement adheres to our policy

No large scale datasets were generated over the course of this study. All relevant data is available in the supplementary material.

Research involving human participants, their data, or biological material

Policy information about studies with human participants or human data. See also policy information about sex, gender (identity/presentation), and sexual orientation and race, ethnicity and racism.

Reporting on sex and gender	Not applicable
Reporting on race, ethnicity, or other socially relevant groupings	Not applicable
Population characteristics	Not applicable
Recruitment	Not applicable
Ethics oversight	Not applicable

Note that full information on the approval of the study protocol must also be provided in the manuscript.

Field-specific reporting

Please select the one below that is the best fit for your research. If you are not sure, read the appropriate sections before making your selection.

☒ Life sciences ☐ Behavioural & social sciences ☐ Ecological, evolutionary & environmental sciences

For a reference copy of the document with all sections, see nature.com/documents/nr-reporting-summary-flat.pdf

Life sciences study design

All studies must disclose on these points even when the disclosure is negative.

Sample size	For microscopy experiments, no sample size calculations were calculated. All analyses were performed on an arbitrarily large number of cells that was representative of the population. Cell chain length quantification was performed on >100 cell chains in three biological replicates. S-layer fractioning experiments involve gel electrophoresis analysis using >10^7 cells at each condition.
Data exclusions	No data excluded.
Replication	All experiments were carried out in at least biological duplicates. For quantitative measurements of microscopy images, at least 5 fields of view were analyzed.
Randomization	We did not randomize samples, as after experimental setup, all measurements and analysis were performed identically across all conditions.
Blinding	We did not blind samples, as after experimental setup, all measurements and analysis were performed identically across all conditions.

Reporting for specific materials, systems and methods

We require information from authors about some types of materials, experimental systems and methods used in many studies. Here, indicate whether each material, system or method listed is relevant to your study. If you are not sure if a list item applies to your research, read the appropriate section before selecting a response.

Materials & experimental systems

n/a	Involved in the study
☐	☒ Antibodies
☒	☐ Eukaryotic cell lines
☒	☐ Palaeontology and archaeology
☒	☐ Animals and other organisms
☒	☐ Clinical data
☒	☐ Dual use research of concern
☒	☐ Plants

Methods

n/a	Involved in the study
☒	☐ ChIP-seq
☒	☐ Flow cytometry
☒	☐ MRI-based neuroimaging

Antibodies

Antibodies used	1) STAR RED maleimide. Cat No: STRED-0003-1MG (1 mM stock solution in DMSO, used at 10 µM). Abberior 2) STAR Green maleimide. Cat No: STGREEN-0003-1MG (1 mM stock solution in DMSO, used at 10 µM). Abberior

3) CF594 maleimide. Cat No: #92025 (1 mM stock solution in DMSO, used at 10 µM). Biotium
4) FluoTag-X2 anti-ALFA (conjugated with Atto488). Cat No: N1502-At488-L (Used at 1:100) NanoTag Biotechnologies.
5) FluoTag-X2 anti-ALFA (conjugated with Alexa647). Cat No: N1502-AF647-L (Used at 1:100) NanoTag Biotechnologies.

Validation

All the dyes and antibodies we used are commercially available.
They were validated using wild-type cells that lack the cys substitution or ALFA tag.
The maleimide-conjugated dyes have also been used by other in previous publications. Specficially, the STAR RED maleimide has been used to label the engineered cysteine-containing S-layer protein in Caulobacter crescentus (doi:10.1038/s41467-019-10650-x). The anti-ALFA antibody conjugated with Atto488 or Alexa647 has also been used to label surface porin proteins in Corynebacterium glutamicum (doi:10.1101/2025.10.14.682376).

Plants

Seed stocks

Not applicable

Novel plant genotypes

Not applicable

Authentication

Not applicable